Int Journ Earth Sciences (1999) 88:422–443

ORIGINAL PAPER

R. Altherr · U. Henes-Klaiber · E. Hegner · M. Satir
C. Langer

Plutonism in the Variscan Odenwald (Germany): from subduction to collision

Received: 7 December 1998 / Accepted: 27 April 1999

Abstract Latest Devonian to early Carboniferous plutonic rocks from the Odenwald accretionary complex reflect the transition from a subduction to a collisional setting. For ~362 Ma old gabbroic rocks from the northern tectonometamorphic unit I, initial isotopic compositions ($\varepsilon_{Nd} = +3.4$ to $+3.8$; $^{87}Sr/^{86}Sr = 0.7035–0.7053$; $\delta^{18}O = 6.8–8.0‰$) and chemical signatures (e.g., low Nb/Th, Nb/U, Ce/Pb, Th/U, Rb/Cs) indicate a subduction-related origin by partial melting of a shallow depleted mantle source metasomatized by water-rich, large ion lithophile element-loaded fluids. In the central (unit II) and southern (unit III) Odenwald, syncollisional mafic to felsic granitoids were emplaced in a transtensional setting at approximately 340–335 Ma B.P. Unit II comprises a mafic and a felsic suite that are genetically unrelated. Both suites are intermediate between the medium-K and high-K series and have similar initial Nd and Sr signatures ($\varepsilon_{Nd} = 0.0$ to –2.5; $^{87}Sr/^{86}Sr = 0.7044–0.7056$) but different oxygen isotopic compositions ($\delta^{18}O = 7.3–8.7‰$ in mafic vs 9.3–9.5‰ in felsic rocks). These characteristics, in conjunction with the chemical signatures, suggest an enriched mantle source for the mafic magmas and a shallow metaluminous crustal source for the felsic magmas. Younger intrusives of unit II have higher Sr/Y, Zr/Y, and Tb/Yb ratios suggesting magma segregation at greater depths. Mafic high-K to shoshonitic intrusives of the southern unit III have initial isotopic compositions ($\varepsilon_{Nd} = -1.1$ to -1.8; $^{87}Sr/^{86}Sr = 0.7054–0.7062$; $\delta^{18}O = 7.2–7.6‰$) and chemical characteristics (e.g., high Sr/Y, Zr/Y, Tb/Yb) that are strongly indicative of a deep-seated enriched mantle source. Spatially associated felsic high-K to shoshonitic rocks of unit III may be derived by dehydration melting of garnet-rich metaluminous crustal source rocks or may represent hybrid magmas.

Key words Odenwald · Mid-German Crystalline Rise · Magmatic arc · Subduction · Granitoid genesis · O–Sr–Nd isotope systematics · High-K granitoids · Monzonitic suite

R. Altherr (✉) · U. Henes-Klaiber · C. Langer
Mineralogisches Institut, Universität Heidelberg,
Im Neuenheimer Feld 236, D-69120 Heidelberg, Germany
Tel.: +49-6221-548206, Fax: +49-6221-544805
e-mail: raltherr@classic.min.uni-heidelberg.de

E. Hegner · M. Satir
Institut für Mineralogie, Petrologie und Geochemie, Universität Tübingen, Wilhelmstrasse 56, D-72074 Tübingen, Germany

Present addresses:
U. Henes-Klaiber, Landesdenkmalamt Baden-Württemberg, Postfach 10 29 37, D-70025 Stuttgart, Germany

C. Langer, Institut für Festkörper- und Werkstofforschung, Helmholtzstrasse 20, D-01069 Dresden, Germany

Introduction

One paramount problem in the interpretation of collisional belts is the spatial and temporal relationship between deformation, metamorphism, magma genesis and magma transport. This is of particular relevance for the European Variscides, where plutonic rocks make up approximately half of the crystalline basement (Finger et al. 1997; Schaltegger et al. 1997). Orogenic granitoid magmas may form by numerous processes in a variety of tectonic settings. It has been suggested that such magmas may evolve from subduction-related basaltic melts through fractional crystallization or assimilation and fractional crystallization (e.g., DePaolo 1981; Hildreth and Moorbath 1988). Alternatively, granitoid magmas may be products of lower crustal dehydration melting of prograde metasedimentary sources (e.g., Patiño Douce and Johnston 1991; Gardien et al. 1995; Patiño Douce and Beard 1996; Thompson 1996; Stevens et al. 1997) or of mafic to intermediate meta-igneous sources (e.g., Atherton and Petford 1993; Rapp 1995; Rapp and Watson 1995; Singh and Johannes 1996).

During the evolution of a collisional belt, material transfer from lower to upper tectonic units by both basal accretion and magma transport seems to be the rule rather than the exception (e.g., Oncken 1997). Within this context, plutonic rocks derived from magmas originally generated at deeper levels provide information on the chemical and physical characteristics of underplated materials and on tectonic and magma-generating processes. In this paper we present a comprehensive set of geochemical and O–Sr–Nd isotope data on latest Devonian to early Carboniferous (~362–335 Ma) plutonic rocks from the Odenwald (Germany) formerly interpreted as part of a deforming early Carboniferous magmatic arc within the European Variscides (Henes-Klaiber et al. 1989; Krohe 1991, 1992, 1996; Oncken 1997) and we use these data to constrain both source compositions and depth ranges of magma generation.

Geological setting

Structural units of the Odenwald

Variscan Europe has been subdivided into numerous zones (Kossmat 1927). Within this traditional frame, the Odenwald forms part of the Mid-German Crystalline Rise (MGCR) within the Saxothuringian zone (Fig. 1). It has been argued that the Saxothuringian zone consists of various units that were derived from a northern lower and a southern upper plate and amalgamated during early Carboniferous oblique convergence (Oncken 1997). In the north of the Saxothuringian zone, low-grade high-pressure/low-temperature metamorphic rock units occurring in the Northern Phyllite Zone and in the southern part of the Rhenohercynian Zone (Fig. 1) document south-directed early Carboniferous subduction processes (Meisl 1970, 1990; Meisl et al. 1982; Ahrendt et al. 1983, 1996; Anderle et al. 1990; Siedel and Theye 1993; Massonne 1995; Ganssloser et al. 1996).

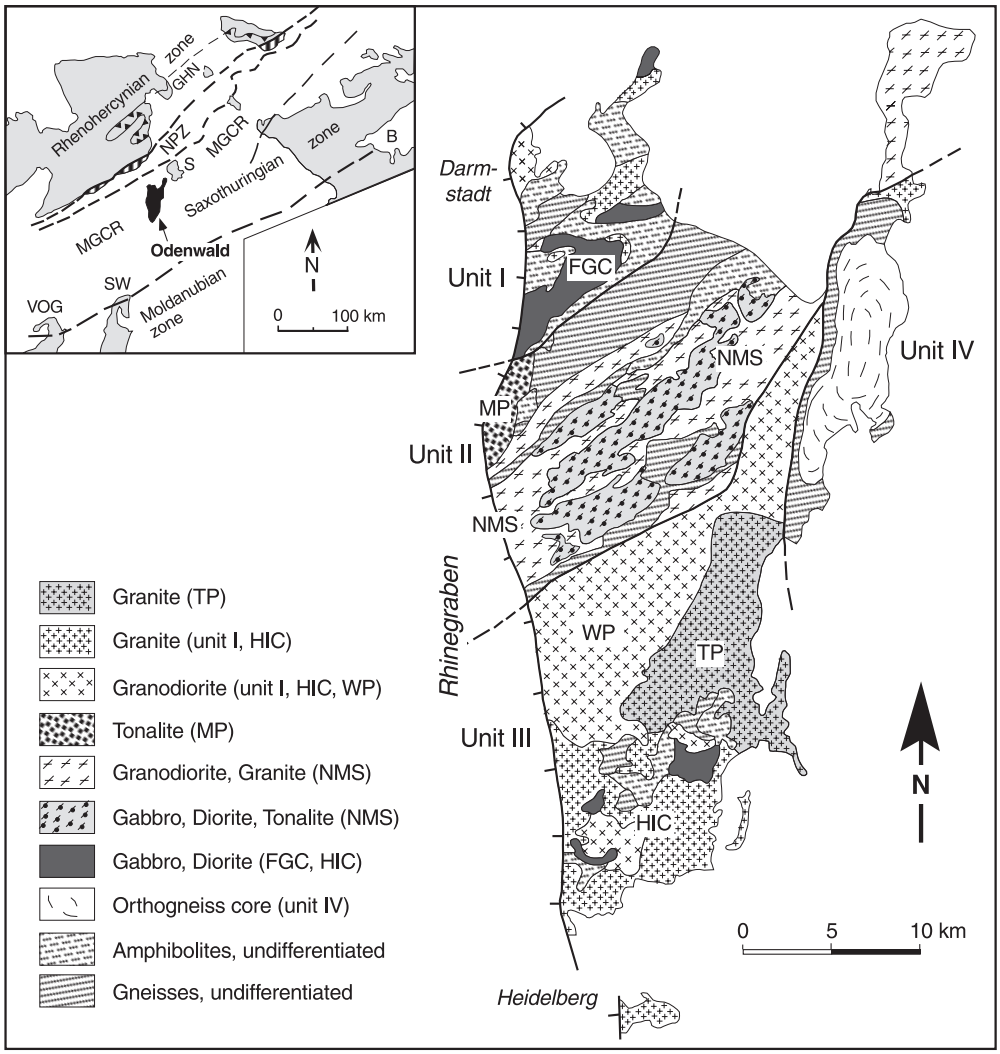

Fig. 1 Simplified map of the Odenwald (modified after Krohe 1996) showing the four major tectonic units (*I–IV*) and intrusive suites. *FGC* Frankenstein gabbroic complex; *HIC* Heidelberg intrusive complex; *MP* Melibokus pluton; *NMS* Neunkirchen magmatic suite; *TP* Tromm pluton; *WP* Weschnitz pluton. *Inset* shows location of the Odenwald complex within the frame of Variscan Europe: *GHN* Giessen-Harz Nappes; *MGCR* Mid-German Crystalline Rise; *NPZ* Northern Phyllite Zone; *B* Barrandian; *S* Spessart; *VOG* Vosges; *SW* Schwarzwald

The Odenwald has been divided into four tectonometamorphic units separated by shear zones (Fig. 1; Krohe 1991, 1992, 1994; Krohe and Willner 1995). Unit I comprises amphibolites and subordinate metapsammitic gneisses equilibrated at approximately 550 °C and 0.15 GPa (Willner et al. 1991; Okrusch 1995). A minimum age for the peak of metamorphism is given by the intrusive emplacement of the Frankenstein gabbroic complex (FGC) at 362 ± 7 Ma B.P. (U–Pb single zircon evaporation; Kirsch et al. 1988). Average $^{40}Ar/^{39}Ar$ hornblende and plagioclase total fusion ages of 363 ± 7 and 359 ± 3 Ma, respectively, imply rapid cooling of the FGC to temperatures below 200 °C (Kirsch et al. 1988). Younger K–Ar ages of 346 ± 4 and 336 ± 4 Ma and of 340 ± 4 and 333 ± 4 Ma were obtained on two hornblende–biotite pairs, respectively, from the granodiorite of Darmstadt (Fig. 1; Kreuzer and Harre 1975, recalculated).

Unit II includes metapsammitic to metapelitic gneisses and subordinate amphibolites, marbles, calcsilicate gneisses, and quartzites (Nickel and Fettel 1985). Reconnaissance studies suggest a clockwise pressure–temperature (P–T) path starting at ≥ 0.6 GPa/ ~ 575 °C and proceeding to 0.5–0.3 GPa/670–610 °C before cooling and exhumation (Willner et al. 1991; Okrusch 1995). Small zircon grains (< 25 μm) from gneisses yielded concordant $^{207}Pb/^{235}U$ and $^{206}Pb/^{238}U$ ages of 336 and 337 Ma, interpreted as the time of peak metamorphic conditions (Todt et al. 1995). Exhumation of the metamorphic rocks was accompained by NE-SW-orientied sinistral strike-slip shearing and contemporaneous intrusion of dioritic to granitic magmas within a transtensional setting (Krohe 1991, 1992, 1996; Krohe and Willner 1995). Compared with the U–Pb zircon ages, the K–Ar ages of hornblende from metamorphic rocks and variably deformed intrusive rocks (374–337 and 345–338 Ma, respectively; with 2-σ errors on individual ages ≈ 4 Ma; Kreuzer and Harre 1975, recalculated) are too high. This is most probably due to variable amounts of inherited (excess) argon. K–Ar ages of biotite from metamorphic and plutonic rocks show considerable scatter (334–325 and 339–327 Ma, respectively; 2-σ errors ≈ 4 Ma; Kreuzer and Harre 1975, recalculated). Hornblende from younger granodioritic dikes cutting both metamorphic and older intrusive rocks yielded K–Ar ages between 338 ± 4 and 330 ± 4 Ma (Kreuzer and Harre 1975, recalculated; Hellmann 1975; Hellmann et al. 1975, 1982).

Unit III contains gneisses that are partially migmatized (Matthes et al. 1972) and include subordinate amphibolites. Due to the lack of suitable mineral assemblages, peak metamorphic conditions are poorly constrained but are thought to have exceeded 650 °C and 4.0 GPa (Willner et al. 1991; Okrusch 1995). Two fine-grained zircon fractions (< 30 μm) from migmatites yielded concordant $^{207}Pb/^{235}U$ and $^{206}Pb/^{238}U$ ages of 342 and 332 Ma (no errors given; Todt et al. 1995). K–Ar cooling ages of hornblende and biotite from voluminous granitoid bodies (quartz diorites, granodiorites, granites; Fig. 1) show only little scatter (336–332 and 329–326 Ma, respectively, with 2-σ errors on individual ages ≈ 4 Ma; Kreuzer and Harre 1975, recalculated; Hellmann et al. 1982), suggesting insignificant contributions of excess argon.

Unit IV forms a NNE-SSW-trending antiform (known as Böllstein Odenwald). Its core is dominated by felsic peraluminous orthogneisses with intercalations of metagabbro and amphibolite. The envelope is composed of paragneisses and amphibolites (Altenberger et al. 1990; Krohe 1991; Altenberger and Besch 1993; Krohe and Willner 1995). A clockwise P–T path was suggested by Willner et al. (1991) and Okrusch (1995) for the rocks from the envelope. Zircon fractions from a paragneiss yielded a U–Pb lower intercept age of 375 ± 2 Ma, interpreted as the time of peak metamorphic conditions (Todt et al. 1995). The protolith age and the age of metamorphism of the orthogneiss core is not well constrained. U–Pb data points of zircon fractions from an orthogneiss sample yielded a poorly defined discordia with an upper intercept age of 354 + 51/–21 Ma and a negative lower intercept age (–40 Ma). Forcing the discordia through the origin yields an upper intercept at 375 Ma (Todt et al. 1995). A Rb–Sr whole-rock "isochron age" of 413 ± 26 Ma (initial $^{87}Sr/^{86}Sr = 0.708 \pm 0.002$) was interpreted as the time of intrusion of the igneous precursors (Lippolt 1986). Reischmann et al. (1999) reported single zircon $^{207}Pb/^{206}Pb$ evaporation ages of 405 ± 3 Ma and interpreted these dates as an approximation of the igneous formation age. Together with similar units in the nearby Spessart (Fig. 1, inset), the orthogneiss core is interpreted as a remnant of an Early Devonian magmatic arc (Altenberger and Besch 1993; Dombrowski et al. 1995; Oncken 1997). Rapid cooling of the complex occurred at ~ 325 Ma B.P. as indicated by scattering K–Ar ages on hornblende, muscovite, and biotite as well as by Rb–Sr mineral/whole-rock ages (Kreuzer and Harre 1975, recalculated; Lippolt 1986). Voluminous late intrusive bodies are lacking.

Accretion of units I–III along NE-trending sinistral shear zones occurred between approximately 340 and 330 Ma B.P. (Krohe and Willner 1995). At that time, unit I had already cooled to temperatures below ~ 200 °C (Kirsch et al. 1988) while the presently exposed levels of units II and III were still at temperatures above ~ 300 °C (i.e., closure temperature for the K–Ar system in biotite). Units II and III are separated from unit IV by a younger NNE-trending WNW-dipping normal fault indicating WNW–ESE extension. This fault was active at approximately 330 Ma B.P. (Hess and Schmidt 1989). Whereas units I to III have been interpreted as relics of a deforming early Carboniferous magmatic arc, unit IV is thought to represent material accreted to the base of the arc during convergence (Oncken 1997).

Intrusive suites: rock types, textures, and modal compositions

The dominant intrusive suite of unit I is the Frankenstein gabbroic complex (FGC) formerly described by Trochim (1955) and Kreher (1994). Rocks of this complex display isotropic textures and, at some localities, brittle deformation. Early magmatic crystallization of plagioclase, clinopyroxene, magnetite, and in some cases also olivine and orthopyroxene was followed by late-stage magmatic growth of ilmenite, apatite, poikilitic brown magnesio-hornblende, and sulfides. Primary igneous textures were modified by subsolidus crystallization of hastingsitic to actinolitic hornblende replacing clinopyroxene, and by subsolidus formation of actinolite and biotite. The dominant rock type in the FGC is hornblende-bearing gabbro. Modal compositions are plagioclase (39–71 vol.%), clinopyroxene (10–24 vol.%), hornblende (2–47 vol.%), magnetite/ilmenite (1–12 vol.%) and include orthopyroxene, biotite, apatite, sulfides, and zircon as accessory phases. Modal layering has been observed at some localities (Kreher 1994, and own observations). The gabbros locally grade into hornblende-clinopyroxene diorites with small amounts of alkalifeldspar, quartz, biotite, and titanite. In the southwestern part of the massif, olivine gabbro and wehrlite are locally abundant. In all rock types plagioclase may be transformed to sericite to varying degrees due to hydrothermal alteration at approximately 140 Ma B.P. (Lippolt and Kirsch 1994).

To the north of the FGC near Darmstadt, a younger granodioritic suite can be mapped in small outcrops and as loose blocks. Because these rocks are heavily weathered, they have not been included in this study.

In unit II numerous small intrusions of gabbroic, dioritic, quartz dioritic, granodioritic, and granitic compositions (Maggetti and Nickel 1973; Nickel and Maggetti 1974; Maggetti 1971, 1974, 1975; Nickel and Fettel 1985) have been collectively termed Neunkirchen magmatic suite (NMS) by Krohe and Willner (1995). Most of these rocks display magmatic and subsolidus foliation planes formed during emplacement into an active NE-trending sinistral shear zone (Krohe 1991). Mafic minerals are mainly hornblende and biotite, with minor clinopyroxene. The occurrence of olivine and orthopyroxene is restricted to gabbronoritic cumulates. Accessory phases are magnetite/ilmenite, apatite, zircon, titanite and allanite.

The Melibokus pluton (MP) located in the western part of unit II is composed of biotite tonalite to granodiorite (Maggetti 1975). The MP was emplaced postkinematically as suggested by its virtually isotropic fabrics. Only in its northern part, near to the contact between units II and I, have deformed varieties been described (Friedrich 1955). Apart from plagioclase, quartz, and alkalifeldspar, the rock contains biotite, titanite, magnetite, apatite, zircon, and allanite as primary minerals.

In unit III three major intrusive complexes are distinguished (Fig. 1). The Weschnitz pluton (WP) is dominated by quartz-bearing biotite-hornblende monzodiorite to granodiorite containing numerous metric to decimetric mafic enclaves (WPE) of quartz dioritic to quartz monzodioritic compositions. Locally, the host rocks are granitic in composition. Rock fabrics are isotropic. In addition to hornblende, biotite, plagioclase, alkalifeldspar, quartz, titanite, magnetite/ilmenite, apatite, and zircon, minor clinopyroxene may occur as relicts in hornblende. The Heidelberg intrusive complex (HIC) is composed of gabbros and diorites intruded by biotite granites and granodiorites ("Schollenagglomerat" of Nickel and Fettel 1985). Mafic minerals are hornblende, clinopyroxene, biotite, magnetite/ilmenite, titanite, apatite, zircon, and allanite. The Tromm pluton (TP) located in the eastern part of unit III is formed by biotite granite containing relatively large amounts of magnetite, titanite, apatite, allanite, and zircon as accessory phases. Granites of the HIC and TP may locally contain secondary muscovite.

In units II and III dikes of granodioritic to granitic compositions cut both the metamorphic and the older intrusive rocks described above (Hellmann 1975; Hellmann et al. 1975, 1982). These rocks are generally undeformed and are referred to as NMSY and HICY further on. As stated above ("Structural units of the Odenwald"), their K–Ar mineral cooling ages are similar to those of the older intrusives.

Analytical techniques

Major elements and the trace elements Rb, Ba, Nb, Sr, Zr, Y, Cr, and Ni were determined by wavelength dispersive X-ray fluorescence (XRF) using standard techniques. For further details see Altherr et al. (1995). The trace elements Cs, Th, U, Ta, Hf, Sc and the REE were determined by instrumental neutron activation analysis (INAA) at Karlsruhe. For details see Class et al. (1994). For the determination of ferrous iron approximately 500 mg sample powder were decomposed in a platinum crucible with a mixture of HF and HSO_4. Crucible and contents were then plunged into boric acid solution and the ferrous iron liberated during the acid decomposition was titrated using potassium permanganate as an indicator. H_2O^+ was determined by Karl-Fischer titration. Carbon dioxide was analyzed by IR gas absorption spectrometry after inductive heating and combustion of the sample in an oxygen atmosphere.

For determination of Sr and Sm–Nd isotope ratios sample powders were decomposed in HF-$HClO_4$ in teflon bombs at 180 °C for 1 week. Sr, Sm, and Nd were separated by conventional ion exchange techniques and analyzed on single W (Sr) and Re (Sm, Nd) double filaments. Total procedure blanks are <100 pg for Sr and <50 pg for Sm and Nd, and they are negligible for the samples of this study. A detailed description of the

analytical procedures is given by Hegner et al. (1995). Isotope ratios were measured on a Finnigan-MAT 262 (Finnigan, Bremen, Germany) multicollector mass spectrometer employing a static mode for Sr and a dynamic multiple mass collection routine for Nd and Sm. Sr isotope ratios are normalized to $^{86}Sr/^{88}Sr = 0.1194$. During the course of this study, four analyses of NBS 987 gave $^{87}Sr/^{86}Sr = 0.710218 \pm 17$ (1 SD), and two analyses of BCR-1 gave $^{87}Sr/^{86}Sr = 0.704972 \pm 10$ (1 SD). Within-run errors (2-σ mean) are less than 0.000015 and external precision (2 σ of population) is estimated to 0.00002. The XRF data with 95% confidence limits of $\pm 3\%$ were used to calculate $^{87}Rb/^{86}Sr$ ratios. Nd isotope ratios are normalized to $^{146}Nd/^{144}Nd = 0.7219$. Measurements of the La Jolla standard provided a mean value of $^{143}Nd/^{144}Nd = 0.511855 \pm 5$ (1 SD; $n = 6$). Furthermore, two analyses of the BCR-1 reference material yielded $^{143}Nd/^{144}Nd = 0.512634 \pm 9$ (1 SD), 6.58 ppm Sm, 28.82 ppm Nd, and $^{147}Sm/^{144}Nd = 0.1382$. Within-run errors on $^{143}Nd/^{144}Nd$ ratios are less than 0.00001 and the external precision is estimated to be better than 0.000015 at the 95% confidence level.

Oxygen for isotope analyses was extracted on a conventional silicate line according to procedures adapted from Venneman and Smith (1990), using BrF_5 as reagent. Samples were reacted at 550 °C. Oxygen yields were commonly between 95 and 100%. The isotopic ratios were measured with a Finnigan MAT 252 mass spectrometer (Finnigan, Bremen, Germany). The ratios are reported in the δ-notion relative to Vienna standard mean ocean water (V-SMOW). Precision is better than $\pm 0.1‰$ based on replicate analyses of an in-house standard (NCSU quartz, $\delta^{18}O = 11.6‰$) and replicate analyses of samples. All values are reported relative to $\delta^{18}O = 9.60‰$ for the quartz standard NBS-28.

Amphibole analyses for Al-in-hornblende barometry were performed using a Camebax SX 50 microprobe (Cameca, Paris, France) equipped with four spectrometers. Operating parameters were 20 s counting time (15 s for Na and K), 10 nA beam current, and 15 kV accelerating voltage. A PAP correction was applied to the data. Natural and synthetic oxide and silicate standards were used for calibration.

Results

Depths of intrusion

Some of the granitoids from the Odenwald contain the critical mineral assemblage hornblende + biotite + plagioclase + alkalifeldspar + quartz + sphene + titanomagnetite + apatite that together with melt is required for application of the Al-in-hornblende barometer (Schmidt 1992). For our pressure estimates, we used rim compositions of hornblende grains in contact with quartz and alkalifeldspar. Cation calculations were based on 23 oxygens and a cation number of 13 excluding Ca, Na, and K.

Table 1 Pressure estimates (± 2-σ errors) for the crystallization of granitoid magmas from the Odenwald obtained from Al-in-hornblende barometry using the calibration of Schmidt (1992)

Sample	Rock type	Pressure (GPa)	Depth (km)[a]
Unit I			
Frankenstein gabbroic complex			
FGC 85	Diorite	0.23 ± 0.12	8.4 ± 4.4
FGC 139	Diorite	0.30 ± 0.06	10.9 ± 2.2
Unit II			
Neunkirchen magmatic suite			
NMS 98	Quartz diorite	0.41 ± 0.12	14.9 ± 4.4
NMS 55	Quartz diorite	0.42 ± 0.06	15.3 ± 2.2
NMS 93	Quartz diorite	0.38 ± 0.14	13.8 ± 5.1
NMS 32	Quartz diorite	0.57 ± 0.18	20.8 ± 6.5
NMS 72	Granite	0.59 ± 0.16	21.5 ± 5.8
Unit III			
Weschnitz pluton			
WP 17	Quartz monzodiorite	0.50 ± 0.04	18.2 ± 1.5
WP 27	Granodiorite	0.49 ± 0.03	17.8 ± 1.1
WPE 20	Quartz diorite	0.50 ± 0.06	18.2 ± 2.2
WPE 25	Quartz diorite	0.45 ± 0.03	16.4 ± 1.1
WPE 26	Quartz diorite	0.51 ± 0.06	18.6 ± 2.2
WPE 111	Quartz diorite	0.48 ± 0.04	17.5 ± 1.5
Heidelberg intrusive complex			
HIC 64	Quartz diorite	0.41 ± 0.03	14.9 ± 1.1
HIC 2	Granite	0.41 ± 0.04	14.9 ± 1.5

[a] Values were calculated assuming an average density of 2.80 g cm^{-3}

Crystallization pressures obtained for the FGC (unit I) range from approximately 0.2 to 0.3 GPa corresponding to a depth of approximately 8–11 km (Table 1). These values are in line with previous estimates based on various mineral equilibria observed in the gabbro and its country rocks (Matthes and Schubert 1971; Maggetti 1975; Willner et al. 1991). Solidification of the NMS magmas (unit II) took place at considerably higher pressures (0.4–0.6 GPa) corresponding to depths between approximately 14 and 22 km (Table 1; note the relatively large errors). Pressure estimates for six samples from the WP (unit III) yielded internally consistent results between 0.45 and 0.51 GPa corresponding to a depth of approximately 17 km. Internally consistent results were also obtained for two different samples from the HIC (~ 0.41 GPa corresponding to ~ 15 km; Table 1).

Whole-rock chemistry

A total of 112 fresh granitoid samples from the different intrusive suites were collected for analysis. Selected chemical analyses of representative samples are given in Table 2. Harker plots show that non-cumulate samples span a continuous range of SiO_2 from approximately 46 to 75 wt.% (Fig. 2), encompassing granitoids, mafic enclaves, and three dykes. Intrasuite chemical variations are very different. The HIC samples, for example, define trends, whereas the NMS

Table 2 Major (wt.%) and trace element (ppm) abundances in representative samples from the Frankenstein gabbroic complex (FGC), Neunkirchen intrusive suite older (NMS) and younger (NMSY) intrusions, Weschnitz pluton host rocks (WP) and mafic enclaves (WPE), Heidelberg intrusive complex older (HIC) and younger (HICY) intrusions, Tromm pluton (TP) and Melibokus pluton (MP)

Unit	FGC	FGC	FGC	FGC	FGC	NMS	NMS	NMS	NMS	NMS
Sample	43	42	85	134	44	73	37	126	125	38
Rock type	G	Hbl-G	D	D	GC	D	QD	QD	Gdr	Gr
SiO_2	50.61	49.87	50.48	49.39	49.79	48.85	54.07	51.38	70.54	70.94
TiO_2	1.00	0.51	0.94	1.19	0.99	1.14	1.46	0.98	0.43	0.25
Al_2O_3	16.28	15.74	19.01	14.66	19.62	18.17	17.90	18.37	15.39	14.08
Fe_2O_3	2.81	1.91	2.39	2.47	2.76	1.83	2.55	1.20	1.04	0.89
FeO	4.93	6.28	4.30	6.78	3.67	7.67	6.01	7.35	2.40	1.71
MnO	0.15	0.16	0.13	0.18	0.12	0.19	0.15	0.17	0.06	0.05
MgO	8.24	8.21	5.87	9.63	5.24	5.68	3.91	5.46	1.15	0.67
CaO	10.45	12.85	10.47	8.19	12.11	10.49	8.10	10.38	3.21	1.41
Na_2O	2.69	1.84	3.42	3.05	3.37	2.90	3.63	2.93	3.85	4.02
K_2O	0.47	0.62	0.85	0.85	0.18	1.00	1.24	1.04	1.74	4.21
P_2O5	0.26	0.04	0.25	0.27	0.33	0.17	0.36	0.17	0.11	0.10
H_2O	1.90	1.78	1.53	2.51	1.10	1.78	1.30	1.27	0.85	0.62
CO_2	0.16	0.14	0.13	0.37	0.13	0.17	0.07	0.06	0.08	0.04
Total	99.95	99.95	99.77	99.54	99.41	100.14	100.75	100.76	100.85	98.99
Mg#	68.6	67.0	64.3	67.9	62.8	54.7	48.3	56.2	40.6	34.6
ASI	0.68	0.58	0.74	0.70	0.71	0.73	0.81	0.74	1.10	1.03
Cr	334	396	240	263	127	88	42	64	14	8
Ni	119	68	64	158	22	8	10	6	<5	<5
Sc	32.3	47.9	29.0	28.8	n.a.	41.6	29.4	38.2	n.a.	7.4
Ga	17	15	20	17	19	22	21	19	19	19
Cs	1.11	5.08	1.73	0.96	n.a.	1.91	1.95	2.09	n.a.	4.88
Rb	10	14	17	19	1	30	36	28	48	136
Sr	897	173	646	416	1516	318	441	299	312	154
Ba	293	110	229	232	230	269	464	244	804	1161
Zr	58	34	81	100	21	91	69	86	209	153
Hf	1.59	0.93	2.41	2.48	n.a.	2.55	2.43	2.55	n.a.	4.90
Nb	5	2	7	8	2	6	7	5	6	11
Ta	0.26	0.05	0.31	0.42	n.a.	0.31	0.50	0.25	n.a.	0.69
Th	0.54	0.62	1.81	1.38	n.a.	0.75	3.21	1.73	n.a.	13.55
U	0.26	0.32	0.71	0.70	n.a.	0.58	1.21	0.73	n.a.	2.60
Y	24	14	25	30	14	32	23	29	17	29
Pb	7	7	8	6	4	8	11	9	13	20
Zn	81	63	70	96	64	100	91	89	68	51
La	15.5	3.7	17.2	17.0	n.a.	13.1	19.3	12.2	n.a.	36.8
Ce	32.6	7.9	38.3	39.3	n.a.	30.7	37.0	31.4	n.a.	69.4
Nd	18.7	5.9	22.8	26.7	n.a.	16.2	24.8	17.4	13.3	29.1
Sm	4.93	1.62	4.86	6.00	n.a.	4.86	4.44	4.28	1.90	6.40
Eu	1.86	0.56	1.52	1.69	n.a.	1.46	1.43	1.33	n.a.	0.98
Gd	5.1	2.1	4.7	5.9	n.a.	5.5	4.4	4.8	n.a.	5.6
Tb	0.79	0.33	0.78	1.01	n.a.	0.88	0.67	0.88	n.a.	0.80
Ho	1.00	0.51	n.a.	1.16	n.a.	1.27	n.a.	1.30	n.a.	n.a.
Tm	0.40	0.20	0.38	0.44	n.a.	n.a.	0.31	0.50	n.a.	0.47
Yb	2.23	1.43	2.34	2.82	n.a.	3.41	1.99	2.95	n.a.	3.03
Lu	0.32	0.21	0.34	0.42	n.a.	0.48	0.27	0.44	n.a.	0.40

For continuation of Table 2 please see the next pages

samples show a relatively large scatter in most variation diagrams. All samples are calc-alkaline (alkali-lime index ≈ 61; not shown). The aluminium saturation index [ASI = molar $Al_2O_3/(CaO + K_2O + Na_2O)$] increases with SiO_2 from approximately 0.6 to 1.17 with all but three samples being characterized by ASI < 1.10 (Fig. 2d). Using the K_2O vs SiO_2 nomenclature of Peccerillo and Taylor (1976), the FGC rocks (unit I) classify as normal calc-alkaline (Fig. 2g). Samples from the NMS (unit II) belong to the normal or high-K calc-alkaline series and unit-III samples display a high-K or even shoshonitic character.

For any given SiO_2, granitoids from tectonic unit III (circular symbols) tend to have higher abundances of K, Rb, Pb, and Sr (Fig. 2g–k), but lower abundances of CaO, Yb, and Sc (Fig. 2e,l,m) than those from units I and II. This tendency is least pronounced for the HIC samples (e.g., Fig. 2k–m). Furthermore, unit-III samples tend to have higher ratios of Sr/Y, Sr/Nd, Zr/Y, and $(Tb/Yb)_{cn}$ (cn = chondrite normalized) than samples from units I and II (Fig. 3). Note that the younger intrusive rocks from unit II (NMSY, MP) show characteristics that are similar to those of the unit-III rocks.

Table 2 continued

Unit	NMS	NMSY	NMS	NMS	NMS	NMS	NMS	MP	WP	WP
Sample	50	74	8	13	12	15	91	68	17	79
Rock type	Gr	GrD	D	DC	QD	Gdr	DC	T	QMD	Gdr
SiO_2	68.08	68.50	52.15	45.44	54.73	71.52	42.43	70.32	60.94	61.95
TiO_2	0.41	0.42	0.79	2.85	1.31	0.25	1.19	0.35	0.89	0.82
Al_2O_3	15.87	15.86	17.51	17.25	18.22	14.36	19.83	15.99	16.94	16.96
Fe_2O_3	1.11	1.40	1.70	3.12	1.87	0.97	3.46	0.76	1.57	1.54
FeO	2.53	0.89	5.75	10.18	6.18	1.46	8.90	1.39	3.17	3.24
MnO	0.07	0.03	0.14	0.24	0.16	0.05	0.16	0.05	0.08	0.08
MgO	0.71	1.09	6.05	5.96	2.70	0.50	8.51	0.79	2.73	2.78
CaO	2.74	1.78	11.43	10.37	7.77	1.97	12.71	2.85	4.90	5.01
Na_2O	4.30	4.72	2.03	1.86	3.19	3.54	1.18	5.04	3.63	3.72
K_2O	3.18	4.09	0.62	0.81	1.44	3.96	0.33	2.57	3.23	2.93
P_2O5	0.13	0.15	0.14	0.20	0.65	0.08	0.03	0.11	0.25	0.24
H_2O	0.73	0.64	1.05	1.39	1.10	0.69	0.85	0.59	1.03	0.88
CO_2	0.11	0.05	0.02	0.16	0.09	0.05	0.11	0.04	0.12	0.06
Total	99.97	99.62	99.38	99.83	99.41	99.40	99.69	100.85	99.48	100.21
Mg#	28.5	50.1	62.2	47.6	40.5	29.8	58.4	43.0	54.1	54.3
ASI	1.02	1.03	0.71	0.76	0.87	1.05	0.78	0.98	0.92	0.92
Cr	14	13	141	51	13	12	123	11	46	44
Ni	<5	<5	22	6	7	<5	17	<5	10	13
Sc	11.1	3.8	39.3	56.3	31.3	6.3	37.4	4.0	10.1	12.1
Ga	20	24	16	21	21	16	20	21	24	23
Cs	1.51	2.13	0.94	1.14	2.69	4.88	1.35	2.07	2.92	4.49
Rb	64	120	15	23	47	117	9	68	105	102
Sr	289	924	333	397	494	215	449	560	797	692
Ba	1758	1880	289	255	527	1518	57	750	1538	1114
Zr	221	172	63	69	77	115	19	119	179	161
Hf	5.63	5.23	1.78	2.63	2.83	3.76	0.53	3.27	6.26	5.37
Nb	10	9	5	8	13	8	2	7	12	11
Ta	0.30	0.69	0.17	0.66	0.82	0.56	0.08	0.44	0.85	0.95
Th	7.08	18.33	2.15	1.70	3.01	19.08	0.40	5.42	13.00	12.08
U	1.12	4.75	0.61	0.69	1.29	2.86	0.15	1.76	3.90	4.06
Y	23	10	18	26	48	15	9	8	16	15
Pb	18	35	10	11	14	33	6	17	26	29
Zn	69	46	67	123	91	42	86	59	74	76
La	58.5	52.5	9.5	18.1	26.4	51.1	3.3	21.4	51.1	44.4
Ce	96.8	97.0	20.4	39.2	63.5	80.2	6.5	35.6	88.4	77.1
Nd	51.8	39.1	11.5	22.2	42.9	27.0	5.2	15.3	42.0	34.0
Sm	7.88	5.71	3.09	5.02	10.25	4.93	1.43	2.43	7.30	5.75
Eu	1.55	1.31	0.95	1.52	2.43	1.00	0.66	0.67	1.87	1.58
Gd	7.0	3.3	3.0	5.6	10.4	3.9	1.7	2.0	6.2	4.6
Tb	0.90	0.49	0.50	0.79	1.66	0.56	0.28	0.25	0.69	0.60
Ho	n.a.	n.a.	0.68	n.a.	1.80	n.a.	n.a.	n.a.	n.a.	n.a.
Tm	n.a.	n.a.	0.27	0.40	n.a.	0.28	0.10	n.a.	0.21	0.25
Yb	1.98	0.74	1.68	2.48	4.03	1.55	0.62	0.55	1.23	1.31
Lu	0.27	0.09	0.23	0.36	0.52	0.22	0.88	0.07	0.17	0.18

The various rock suites are most readily distinguished by means of a Rb vs Sr diagram (Fig. 4). For any given Sr content, the rocks from units I and II (with the exception of the NMSY samples) are characterized by Rb abundances that are lower than those of unit-III rocks. Moreover, the different suites from unit III and the NMSY define different fractionation trends. Weschnitz pluton and WPE samples, however, show a relatively large scatter.

Chondrite-normalized rare earth element (REE) patterns of the FGC rocks (unit I) are characterized by low $(La/Yb)_{cn}$ ratios and the absence of a significant Eu anomaly (Fig. 5a). Non-cumulate NMS rocks (unit II) show variable internal fractionation of the REE, whereby there is only a weak tendency for $(La/Yb)_{cn}$ and $(Tb/Yb)_{cn}$ values to increase from the diorites and quartz diorites to granodiorites and granites (Fig. 5b–e). The magnitude of the negative Eu anomaly does not depend on the bulk composition. A common feature of the REE patterns of unit-III samples (excluding some of the WPE rocks) is the absence of a pronounced negative Eu anomaly (Fig. 5f–i). With the exception of the HIC samples, $(Tb/Yb)_{cn}$ values of unit-III rocks are considerably higher than those of the NMS samples (Fig. 3c). The younger intrusives from units II and III (NMSY, HICY) show the highest $(Tb/Yb)_{cn}$ values and have no Eu anomaly (Figs. 3c, 5j,k).

Nd–Sr–O isotope ratios

Nd, Sr, and O isotope data are listed in Table 3. Initial Sr and Nd isotopic compositions were calculated for

Table 2 continued

Unit	WP	WP	WPE	HIC	HIC	HIC	HICY	HICY	TP	TP
Sample	27	24	19	64	77	1	62	63	66	67
Rock type	Gdr	Gr	QMD	QD	Gdr	Gr	GdrD	GrD	Gr	Gr
SiO_2	61.76	71.64	53.84	51.91	64.87	69.96	66.28	70.79	69.99	68.03
TiO_2	0.86	0.31	0.98	1.22	0.52	0.36	0.61	0.38	0.32	0.44
Al_2O_3	17.26	14.60	16.08	17.84	15.32	14.90	16.70	15.27	15.54	16.28
Fe_2O_3	1.39	0.76	2.47	1.95	1.25	1.36	1.43	0.70	1.04	1.45
FeO	2.95	1.20	4.59	6.13	2.96	1.12	1.58	1.16	0.71	1.02
MnO	0.06	0.02	0.16	0.15	0.07	0.07	0.04	0.03	0.03	0.04
MgO	2.44	0.81	5.18	4.95	2.62	1.34	1.54	0.81	0.78	1.15
CaO	4.81	2.21	6.77	8.98	4.18	1.99	2.33	1.70	1.62	1.62
Na_2O	3.98	3.07	3.20	3.29	2.85	3.80	4.42	3.68	4.18	4.54
K_2O	3.05	4.75	4.05	1.69	3.77	4.08	4.16	4.68	4.51	4.24
P_2O_5	0.27	0.11	0.41	0.27	0.22	0.12	0.23	0.14	0.11	0.15
H_2O	0.75	0.66	1.03	1.42	1.13	0.65	0.82	0.61	0.72	0.88
CO_2	0.06	0.04	0.08	0.07	0.07	0.23	0.32	0.27	0.52	0.22
Total	99.64	100.18	98.94	99.87	99.83	99.98	100.46	100.22	100.07	100.06
Mg#	53.5	46.0	60.1	55.4	56.0	53.1	51.5	47.3	48.4	49.5
ASI	0.93	1.03	0.73	0.76	0.94	1.04	1.04	1.07	1.06	1.09
Cr	39	11	154	108	72	18	19	13	12	14
Ni	13	<5	59	29	19	6	<5	<5	<5	6
Sc	8.9	0.8	18.3	29.8	11.6	4.2	5.8	4.3	3.6	n.a.
Ga	25	18	22	22	18	19	26	24	23	24
Cs	2.44	2.62	1.74	3.83	5.32	7.93	4.82	8.41	6.65	n.a.
Rb	92	116	94	64	137	150	139	177	157	125
Sr	972	697	732	458	450	340	799	450	735	1028
Ba	1536	1945	2230	622	1055	1322	1667	1180	1967	2424
Zr	174	132	197	131	137	123	212	159	133	184
Hf	4.82	3.66	5.67	4.24	4.12	3.92	6.14	4.87	4.61	n.a.
Nb	11	5	15	10	10	12	11	13	8	10
Ta	0.87	0.50	0.70	0.53	0.51	0.81	0.87	0.72	0.61	n.a.
Th	14.63	12.48	16.40	4.29	30.38	19.37	17.62	21.11	21.01	n.a.
U	3.70	2.39	3.10	1.46	5.54	3.40	2.37	2.57	3.33	n.a.
Y	13	6	23	28	19	15	11	12	8	14
Pb	26	34	28	15	23	32	32	46	40	35
Zn	76	35	110	82	53	49	70	46	48	64
La	66.4	39.2	72.9	23.2	48.7	38.3	85.7	49.8	52.9	n.a.
Ce	112.9	56.4	119.0	48.1	82.7	60.7	134.0	87.9	81.2	n.a.
Nd	53.4	17.1	55.5	27.1	30.4	24.2	53.3	35.5	29.2	52.3
Sm	9.19	2.83	9.42	5.87	5.47	4.08	7.80	5.85	4.52	7.51
Eu	1.75	0.61	2.21	1.70	1.20	0.90	1.81	1.21	1.16	n.a.
Gd	5.0	1.7	5.9	6.2	5.0	2.9	6.2	3.9	3.4	n.a.
Tb	0.56	0.26	0.92	0.85	0.68	0.47	0.62	0.51	0.30	n.a.
Ho	n.a.	0.33	n.a.	1.10	0.85	n.a.	n.a.	0.48	n.a.	n.a.
Tm	n.a.	0.10	0.40	n.a.	0.29	0.21	0.21	n.a.	0.10	n.a.
Yb	1.05	0.44	1.78	2.40	1.71	1.13	0.73	0.51	0.56	n.a.
Lu	0.14	0.05	0.26	0.33	0.25	0.16	0.09	0.05	0.07	n.a.

Rock types: gabbroic cumulate (GC); gabbro (G); hornblende gabbro (Hbl-G); dioritic cumulate (DC); diorite (D); quartz diorite (QD); quartz monzodiorite (QMD); tonalite (T); granodiorite (Gdr); granite (Gr); granodioritic dike (GdrD); and granitic dike (GrD). ASI is the aluminium saturation index [molar $Al_2O_3/(CaO+K_2O+Na_2O)$] and Mg# is $100\times$molar $MgO/(MgO+0.9FeO_{total})$. See text for analytical techniques

ages of 360 Ma (FGC), 340 Ma (NMS), and 335 Ma (WP, HIC, TP, MP, NMSY, HICY). These ages approximate the respective time of emplacement quite well (see constraints given in "Structural units of the Odenwald"). Because Rb/Sr and Sm/Nd ratios are generally low (Table 3), even a difference of 10 Ma would not significantly change the calculated intial isotopic values. Figure 6a shows the variation of initial ε_{Nd} values with initial $^{87}Sr/^{86}Sr$ isotope ratios. Taken as a whole, the samples show a weak negative correlation between both parameters, whereby average $\varepsilon_{Nd}(I)$ values decrease and $^{87}Sr/^{86}Sr(I)$ values increase from unit I to unit III. The FGC samples (unit I) show nearly constant $\varepsilon_{Nd}(I)$ with increasing $^{87}Sr/^{86}Sr(I)$. Note that the younger intrusives MP (unit II) and HICY (unit III) have $\varepsilon_{Nd}(I)$ and $^{87}Sr/^{86}Sr(I)$ values that form the end members of the variation trend defined by samples of units II and III.

As none of the samples chosen for isotope analyses show petrographic evidence for hydrothermal metamorphism, such as chloritization of biotite or formation of sericite from plagioclase, measured $\delta^{18}O$ values are thought to reflect primary oxygen isotopic compositions. Samples from the FGC (unit I) display a positive

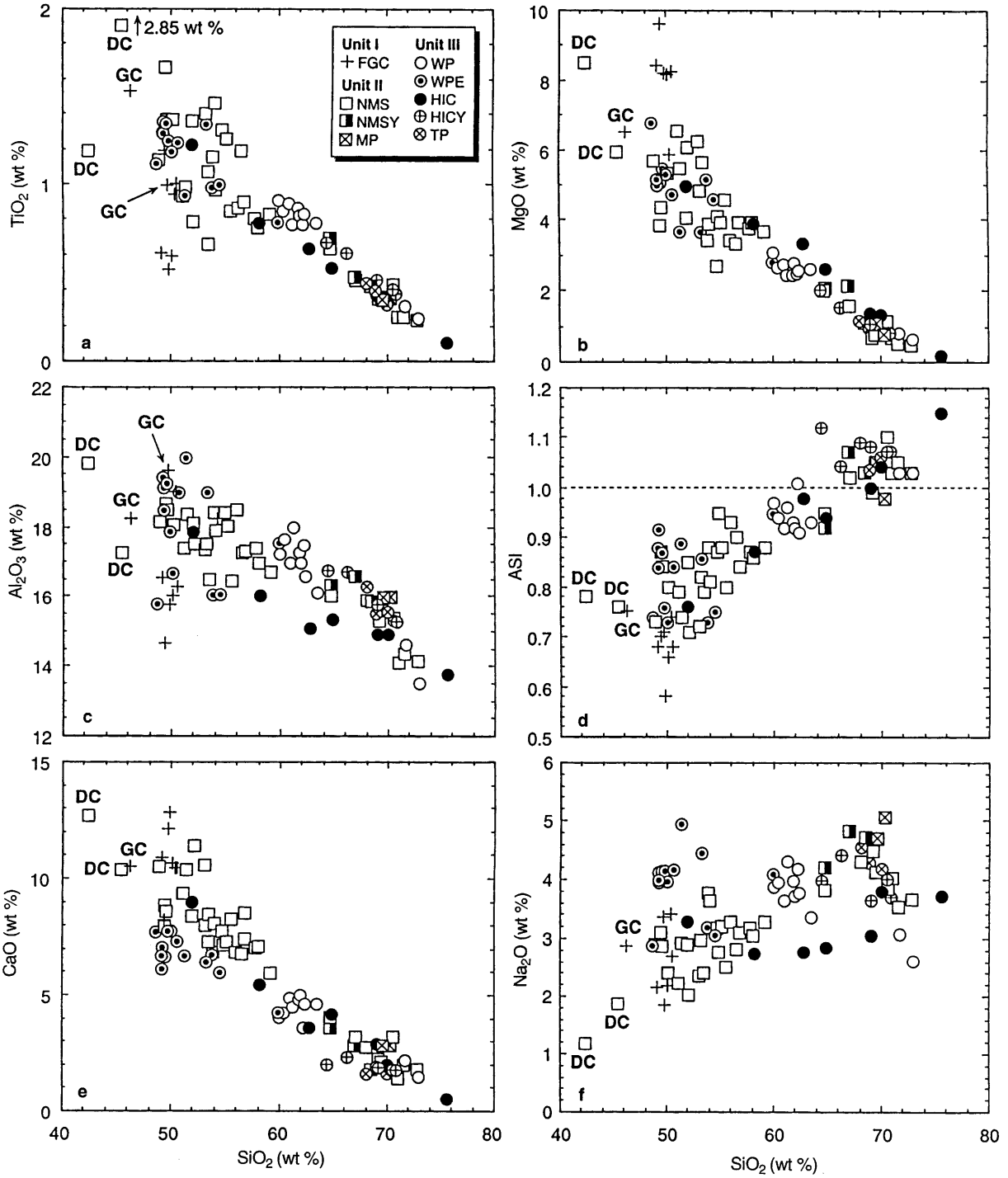

Fig. 2a–m Selected Harker variation diagrams for granitoids from the Odenwald illustrating some of the chemical features that distinguish intrusive suites from the different structural units I–III. *DC* dioritic cumulate; *GC* gabbroic cumulate. Dashed reference line in **d** separates metaluminous (ASI < 1.0) from peraluminous (ASI > 1.0) compositions. The diagram of K_2O vs SiO_2 (**g**) shows field boundaries between calc-alkaline (medium-K), high-K and shoshonitic series of Peccerillo and Taylor (1976)

correlation between $\delta^{18}O$ and $^{87}Sr/^{86}Sr(I)$ values (Fig. 6). Such a relationship, however, is not observed with samples from units II and III, $\delta^{18}O$ showing a large variation and no correlation with $^{87}Sr/^{86}Sr(I)$. Samples from individual structural units do not show any systematic variation of both $\varepsilon_{Nd}(I)$ and $^{87}Sr/^{86}Sr(I)$ with SiO_2 (Fig. 6c,d). Positive correlations do, however, exist between $\delta^{18}O$ and SiO_2 (Fig. 6e). It is important to note that the MP sample (unit II) has a significantly lower $\delta^{18}O$ value compared with samples with similar SiO_2 from the other units.

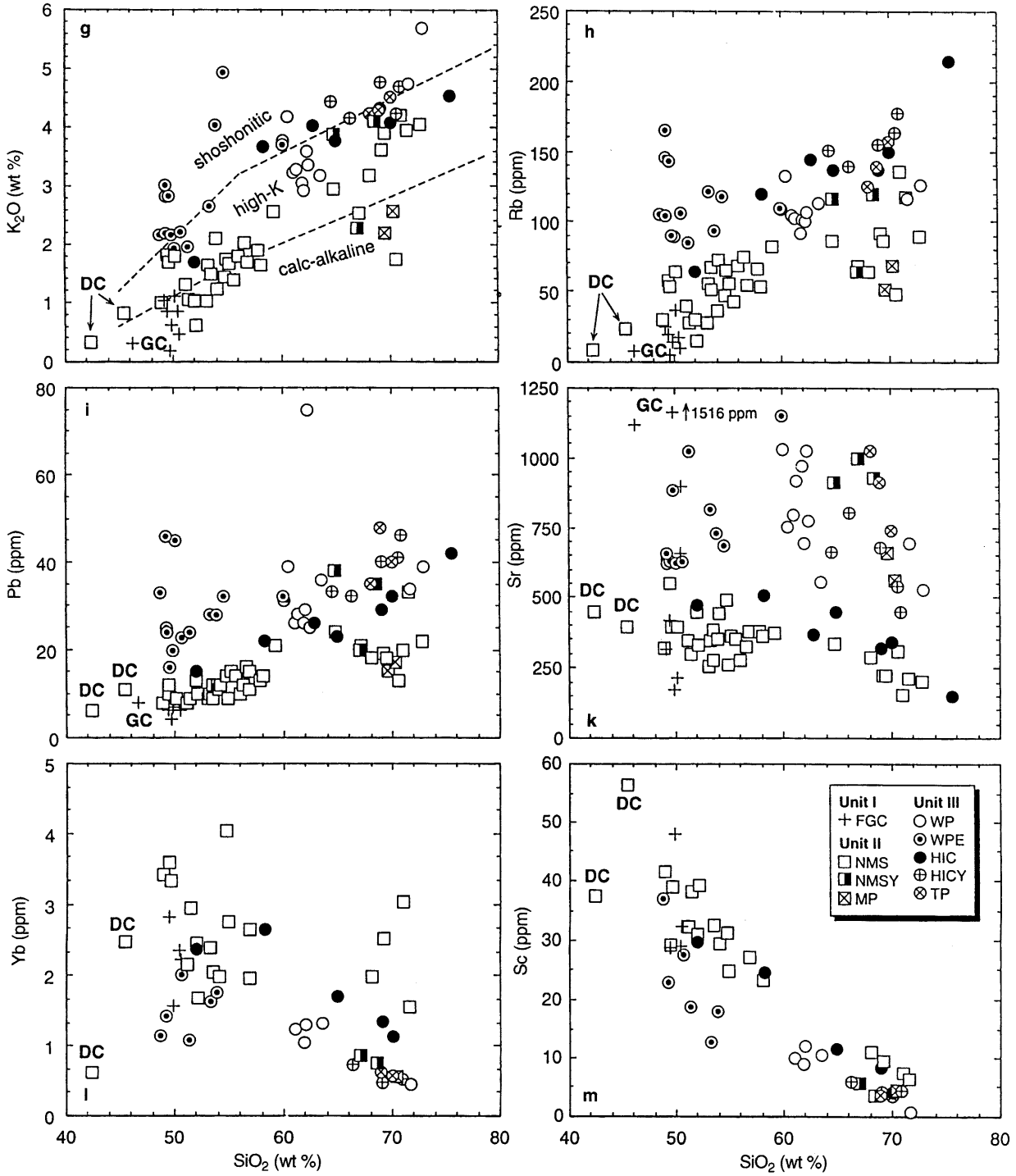

Fig. 2 Continued

Discussion

Mantle origin of FGC magmas

Non-cumulate gabbroic and dioritic rocks from the FGC (unit I) display high values of Mg# [$=100\times$molar MgO/(MgO + 0.9FeO$_{tot}$)] (68 to 47; Table 2), MgO (9.6 to 5.2 wt.%), CaO (12.8 to 7.4 wt.%), Cr (396 to 46 ppm), and Ni (158 to 21 ppm). These characteristics indicate an origin from variably fractionated mantle melts. Numerous chemical features, such as relatively low abundances of K_2O (0.31–1.09%), Rb (7–36 ppm), Ba (110–293 ppm), LREE (e.g., La = 3.7–17.2 ppm), Zr (34–100 ppm), and Hf (0.93–2.48 ppm), high ratios of K/Rb (415–251), La/Nb (3.1–1.9), and Hf/Ta (6.1–18.6), but low ratios of Nb/Th (9.3–3.2), Nb/U (19.2–9.8), Ce/Pb (6.6–1.1), Th/U (1.94–2.55), and Rb/Cs

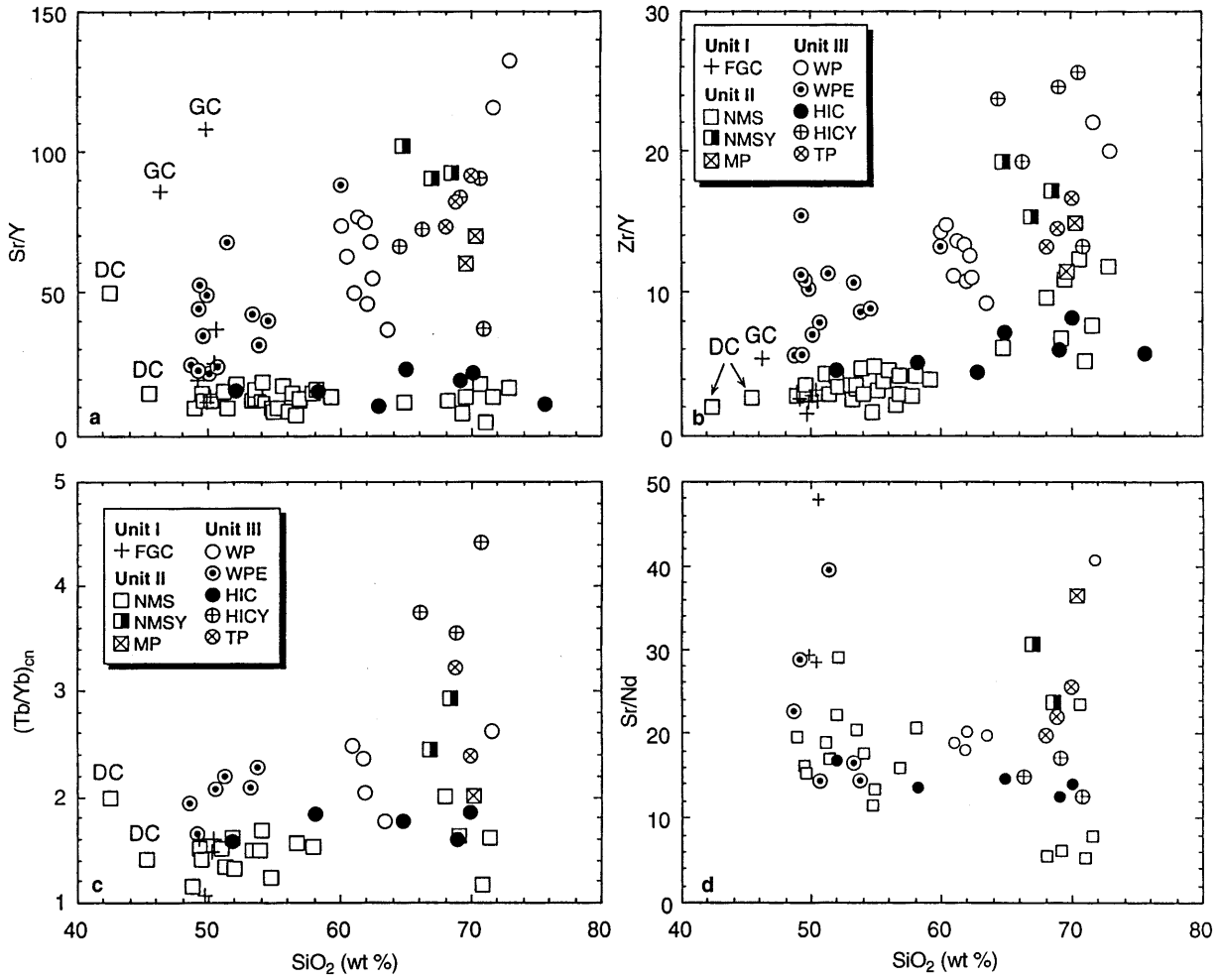

Fig. 3a–d Variation of Sr/Y, Zr/Y, $(Tb/Yb)_{cn}$ and Sr/Nd ratios with SiO_2 in the Odenwald plutonic suites

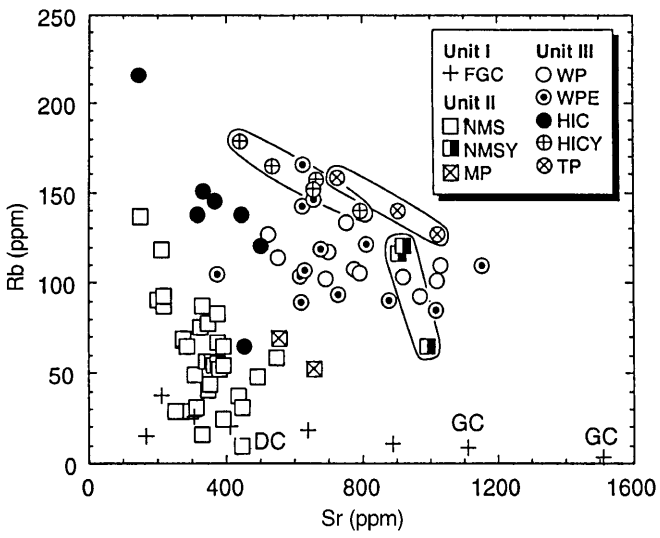

Fig. 4 Rb vs Sr relationships of the Odenwald granitoid suites. Note that samples from unit-III and the younger unit-II suites have higher Rb and Sr than the older unit-II and unit-I rocks. Different suites from unit III and the NMSY samples show different fractionation trends

(2.8–21.4), suggest a subduction-related origin. Enrichment of U relative to Th, for example, may be caused by the addition of slab-derived fluids to the magma sources (e.g., Keppler 1996). An overabundance of Cs relative to Rb and K is observed in all arc suites and is commonly attributed to the contribution of Cs-enriched pelagic sediments which have a Rb/Cs range of approximately 10–30 (e.g., White and Dupré 1986; Hart and Reid 1991) as opposed to average values of 53 and 30 for the lower and upper crust, respectively (Taylor and McLennan 1985). Isotopic parameters (Fig. 5; Table 3), i.e., relatively high ε_{Nd} values between +3.8 and +3.4, as well as relatively low values of $^{87}Sr/^{86}Sr(I)$ (0.7033 to 0.7046) and $\delta^{18}O$ (6.8–7.9‰), are also consistent with an arc-related origin of the FGC magmas, without significant contributions of material from the overlying crust.

Chondrite-normalized REE patterns of FGC rocks (unit I) are relatively flat and do not show significant Eu anomalies (Fig. 5a). Furthermore, these rocks are characterized by relatively high abundances of Sc and HREE (Fig. 2l,m) as well as by low Zr/Y, Sr/Y, and $(Tb/Yb)_{cn}$ values (Fig. 3a–c). These signatures together with the isotopic parameters (Fig. 6; Table 3) are consistent with a derivation of these magmas from a

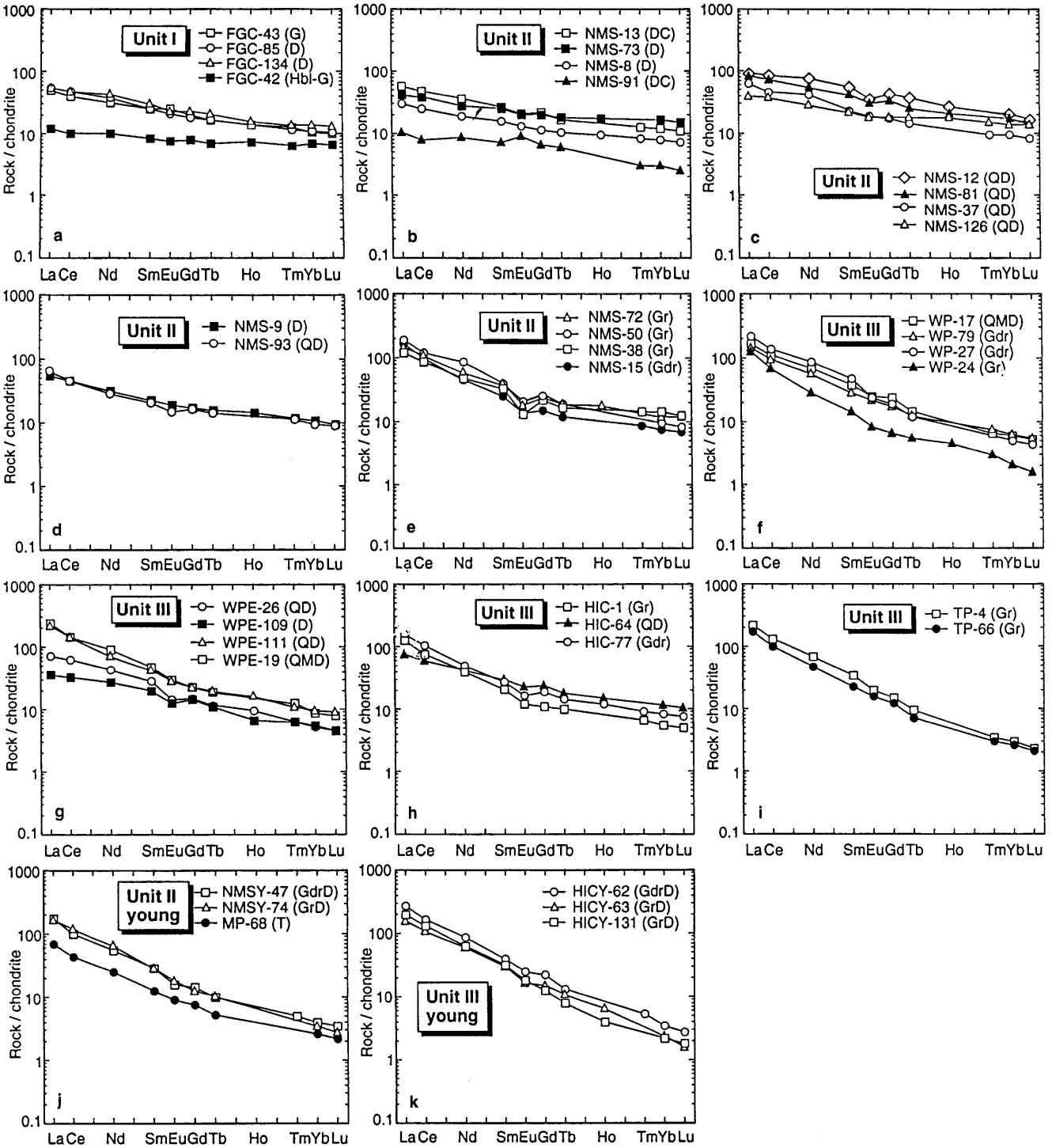

Fig. 5a–k Chondrite-normalized REE abundance patterns (normalized to values given in Boynton 1984) for selected samples of the different intrusive suites. **a** Frankenstein gabbroic complex (*FGC*): gabbro (*G*); hornblende gabbro (*Hbl-G*); diorite (*D*). **b** Neunkirchen magmatic suite (*NMS*): diorite (*D*); dioritic cumulate (*DC*). **c** Neunkirchen magmatic suite (*NMS*): quartz diorite (*QD*). **d** Neunkirchen magmatic suite (*NMS*): quartz diorite (*QD*); diorite (*D*). **e** Neunkirchen magmatic suite (*NMS*): granodiorite (*Gdr*); granite (*Gr*). **f** Weschnitz pluton (*WP*): quartz monzodiorite (*QMD*); granodiorite (*Gdr*); granite (*Gr*). **g** Weschnitz pluton, mafic enclaves (*WPE*): quartz diorite (*QD*); quartz monzodiorite (*QMD*); diorite (*D*). **h** Heidelberg intrusive complex (*HIC*): quartz diorite (*QD*); granodiorite (*Gdr*); granite (*Gr*). **i** Tromm pluton (*TP*): granite (*Gr*); **j** Younger intrusives in unit II (*NMSY, MP*): tonalite (*T*), granitic dike (*GrD*); **k** Younger intrusives in unit III (*HICY*): granodioritic dike (*GdrD*), granitic dike (*GrD*)

garnet-free spinel-peridotitic mantle metasomatized by slab-derived fluids.

Genesis of unit-II magmas

As for mafic compositions Mg# shows more variation than SiO_2, the abundances of some oxides and elements in the non-cumulate NMS samples have been plotted in variation diagrams with Mg# on the abscissa (Fig. 7). It is evident that the NMS comprises at least two groups of rocks characterized by different fractionation behavior. Despite some scatter, the mafic rocks (diorites and quartz diorites) form relatively coherent trends whereby Al_2O_3, TiO_2, P_2O_5, Sr, Nb, La, Yb, Eu, and Y increase, but MgO and CaO decrease with decreasing Mg#. For most elements (e.g., TiO_2, P_2O_5, Sr, Nb, Yb, Eu, Y), the felsic rocks (granodiorites and granites) do not follow these trends. Such behavior rules out a comagmatic relationship of felsic and mafic NMS rocks.

Mafic non-cumulate NMS rocks (diorites and quartz diorites) are characterized by relatively high Mg# (69 to 40) and low Na_2O contents (<3.8 wt.%). Several experimental studies (e.g., Wolf and Wyllie 1994; Rapp 1995; Rapp and Watson 1995) have shown that extremely high temperatures in excess of $\sim 1100\,^{\circ}C$ are needed to produce mafic meta-aluminous low-silica (<58 wt.%) melts by dehydration melting of metabasic crustal rocks. In marked contrast to the mafic NMS rocks, such melts are generally characterized by low Mg# (<44) and high contents of Na_2O (>4.3wt%). Therefore, an intracrustal origin of the mafic NMS magmas is unlikely and we favor a derivation from a mantle source.

Isotopic characteristics of mafic NMS samples, such as $\varepsilon_{Nd}(I)$ values between 0.0 and –1.5, $^{87}Sr/^{86}Sr(I)$ values between 0.7050 and 0.7053, and $\delta^{18}O$ values between 7.4 and 8.6‰ (Fig. 6c–e; Table 3), suggest an enriched rather than a depleted mantle source for the mafic NMS magmas. This is in marked contrast to the older, subduction-related FGC magmas, for which a more depleted mantle source is proposed. High abundances of Yb and Sc (Fig. 2l,m) and low ratios of Sr/Y, Zr/Y, and $(Tb/Yb)_{cn}$ (Figs. 3a–c, 5b–d) suggest a spinel peridotite, rather than a garnet peridotite, source.

As the mafic and felsic NMS rocks are genetically unrelated, an origin by dehydration melting of crustal source rocks has to be considered for the latter. Compositional diversity among crustal-derived magmas may arise from both different source compositions and variation of melting conditions such as pressure and temperature (e.g., Beard et al. 1994; Wolf and Wyllie 1994; Patiño Douce and Beard 1995, 1996; Patiño Douce 1996; Thompson 1996; Stevens et al. 1997, and references therein). Compositional differences of magmas produced by partial melting of different source rocks, such as amphibolites, metagraywackes, and metapelites, under variable melting conditions, may be visualized in terms of molar oxide ratios such as $Al_2O_3/(MgO+FeO_{total})$, K_2O/Na_2O and $CaO/(MgO+FeO_{total})$. Partial melts derived from mafic sources, for example, have lower K_2O/Na_2O and $Al_2O_3/(MgO+FeO_{total})$, but higher $CaO/(MgO+FeO_{total})$ than those derived from metapelites (Fig. 8). The felsic NMS rocks plot into the low-$Al_2O_3/(MgO+FeO_{total})$

Table 3 Sm–Nd, Rb–Sr and O isotope data for Odenwald granitoids. $^{87}Rb/^{86}Sr$ values were calculated from XRF data. Initial ε_{Nd} values [$\varepsilon_{Nd}(I)$] and initial Sr isotope ratios [$^{87}Sr/^{86}Sr(I)$] are based on 360 Ma (FGC), 340 Ma (NMS) and 335 Ma (WP, HIC, HICY, TP, MP). $\delta^{18}O$ values are relative to V-SMOW. For rock types see Table 2. For errors see "Analytical techniques"

Sample	Sm (ppm)	Nd (ppm)	$^{147}Sm/^{144}Nd$	$^{143}Nd/^{144}Nd$	ε_{Nd} (I)	$^{87}Rb/^{86}Sr$	$^{87}Sr/^{86}Sr$	$^{87}Sr/^{86}Sr$ (I)	$\delta^{18}O$ (‰)
FGC-42	1.62	5.90	0.1665	0.512743	+3.5	0.23	0.704448	0.7033	6.86
FGC-85	4.86	22.78	0.1289	0.512651	+3.4	0.076	0.704429	0.7040	7.53
FGC-134	6.00	q26.70	0.1358	0.512686	+3.8	0.13	0.705315	0.7046	7.97
FGC-44	3.03	12.48	0.1467	0.512709	+3.7	0.002	0.703503	0.7035	6.83
NMS-37	4.44	24.83	0.1080	0.512439	0.0	0.24	0.706412	0.7052	8.65
NMS-126	4.28	17.38	0.1488	0.512514	−0.3	0.27	0.706354	0.7050	7.42
NMS-125	1.90	13.32	0.08638	0.512312	−1.5	0.44	0.707708	0.7055	9.52
NMS-50	7.88	51.77	0.09201	0.512280	−2.4	0.64	0.707508	0.7044	9.35
NMS-13	5.02	22.23	0.1366	0.512372	−2.5	0.17	0.706380	0.7055	7.27
NMS-12	10.25	42.87	0.1446	0.512443	−1.5	0.28	0.706702	0.7053	8.03
NMS-91	1.43	5.18	0.1664	0.512464	−2.1	0.06	0.705859	0.7056	7.81
WP-79	5.75	34.04	0.1021	0.512298	−2.6	0.426	0.708227	0.7062	7.80
WP-27	9.19	53.39	0.1041	0.512335	−1.9	0.274	0.709109	0.7078	8.12
WPE-19	9.42	55.48	0.1027	0.512338	−1.8	0.37	0.707983	0.7062	7.62
HIC-64	5.87	27.07	0.1310	0.512439	−1.1	0.40	0.707318	0.7054	7.25
HIC-77	5.47	30.36	0.1089	0.512272	−3.4	0.881	0.710952	0.7068	8.49
HIC-1	4.08	24.20	0.1019	0.512314	−2.3	1.28	0.711675	0.7056	9.07
HICY-62	7.80	53.27	0.08854	0.512197	−4.0	0.503	0.709075	0.7066	9.50
HICY-63	5.85	35.47	0.09973	0.512229	−3.8	1.14	0.712274	0.7068	9.95
TP-67	7.51	52.31	0.08682	0.512221	−3.5	0.352	0.707872	0.7062	9.97
MP-68	2.43	15.28	0.09627	0.512463	+0.8	0.351	0.706367	0.7047	8.02

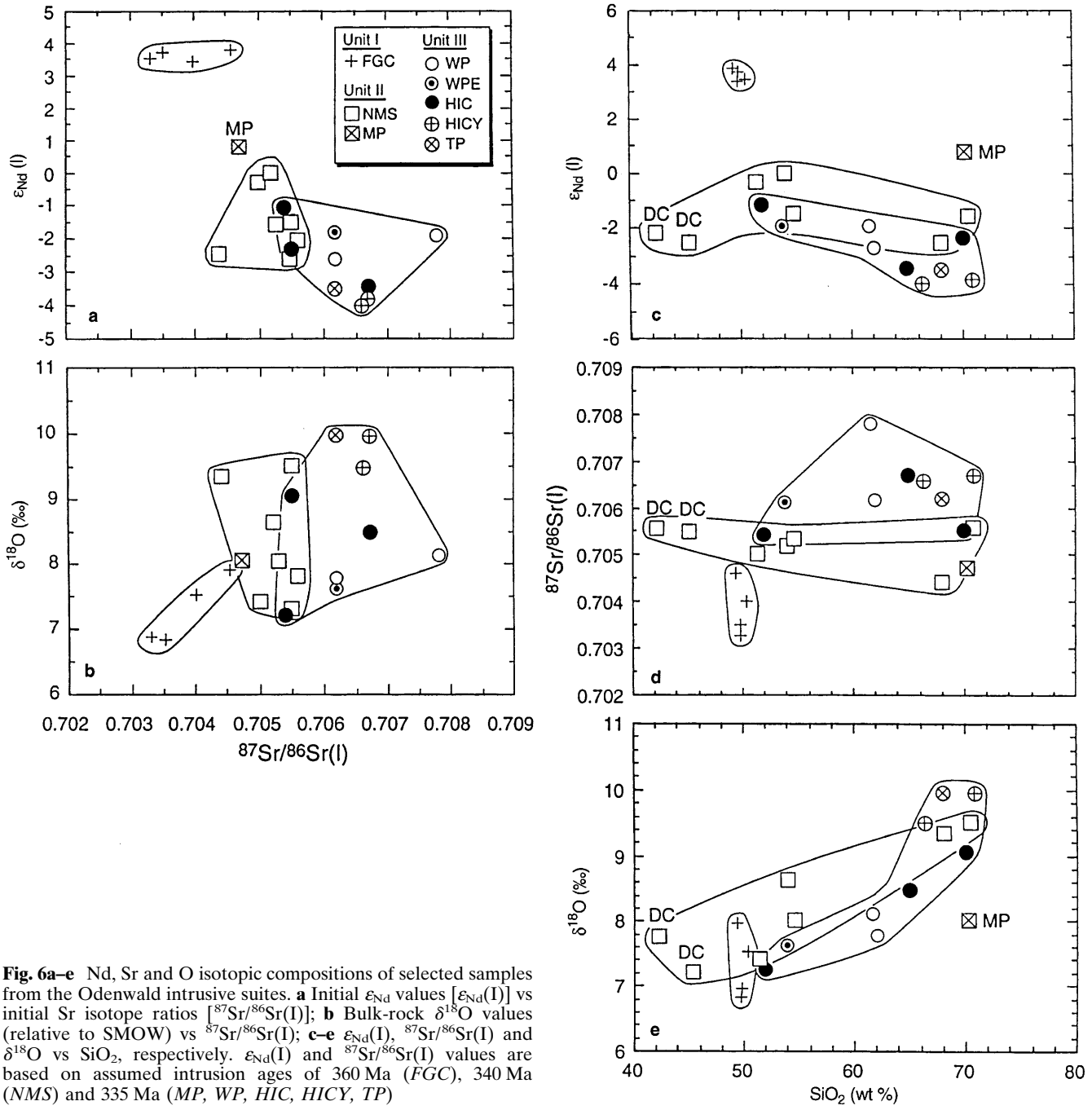

Fig. 6a–e Nd, Sr and O isotopic compositions of selected samples from the Odenwald intrusive suites. **a** Initial ε_{Nd} values [ε_{Nd}(I)] vs initial Sr isotope ratios [$^{87}Sr/^{86}Sr$(I)]; **b** Bulk-rock $\delta^{18}O$ values (relative to SMOW) vs $^{87}Sr/^{86}Sr$(I); **c–e** ε_{Nd}(I), $^{87}Sr/^{86}Sr$(I) and $\delta^{18}O$ vs SiO_2, respectively. ε_{Nd}(I) and $^{87}Sr/^{86}Sr$(I) values are based on assumed intrusion ages of 360 Ma (*FGC*), 340 Ma (*NMS*) and 335 Ma (*MP, WP, HIC, HICY, TP*)

part of the field for partial melts from metagraywackes. Whereas an origin from a mixed metabasaltic/metagraywacke source also seems possible, metapelitic sources can safely be excluded because all samples have high $CaO/(MgO+FeO_{total})$ ratios.

Important constraints on the depth of magma segregation may be obtained from trace element characteristics. Crustal lithologies show a depth-dependent mineralogy. For any fixed bulk-rock composition the amount of garnet increases and the amount of plagioclase decreases with increasing depth. Certain trace element abundances and ratios may be used as indicators for the relative amounts of garnet, plagioclase, and hornblende as fractionating phases during either magma segregation or differentiation. Fractionation of garnet will lower the relative abundances of HREE, Y, and Sc in the remaining melt phase. Plagioclase fractionation will result in low relative abundances of Ba and Sr, low Sr/Nd ratios, and negative Eu anomalies in the chondrite-normalized REE patterns of the melts. Fractionation of hornblende will cause an increase in LREE/HREE in the residual melt, but the resulting chondrite-normalized REE pattern of the melt should be characterized by a concave-upward shape (e.g., Romick et al. 1992).

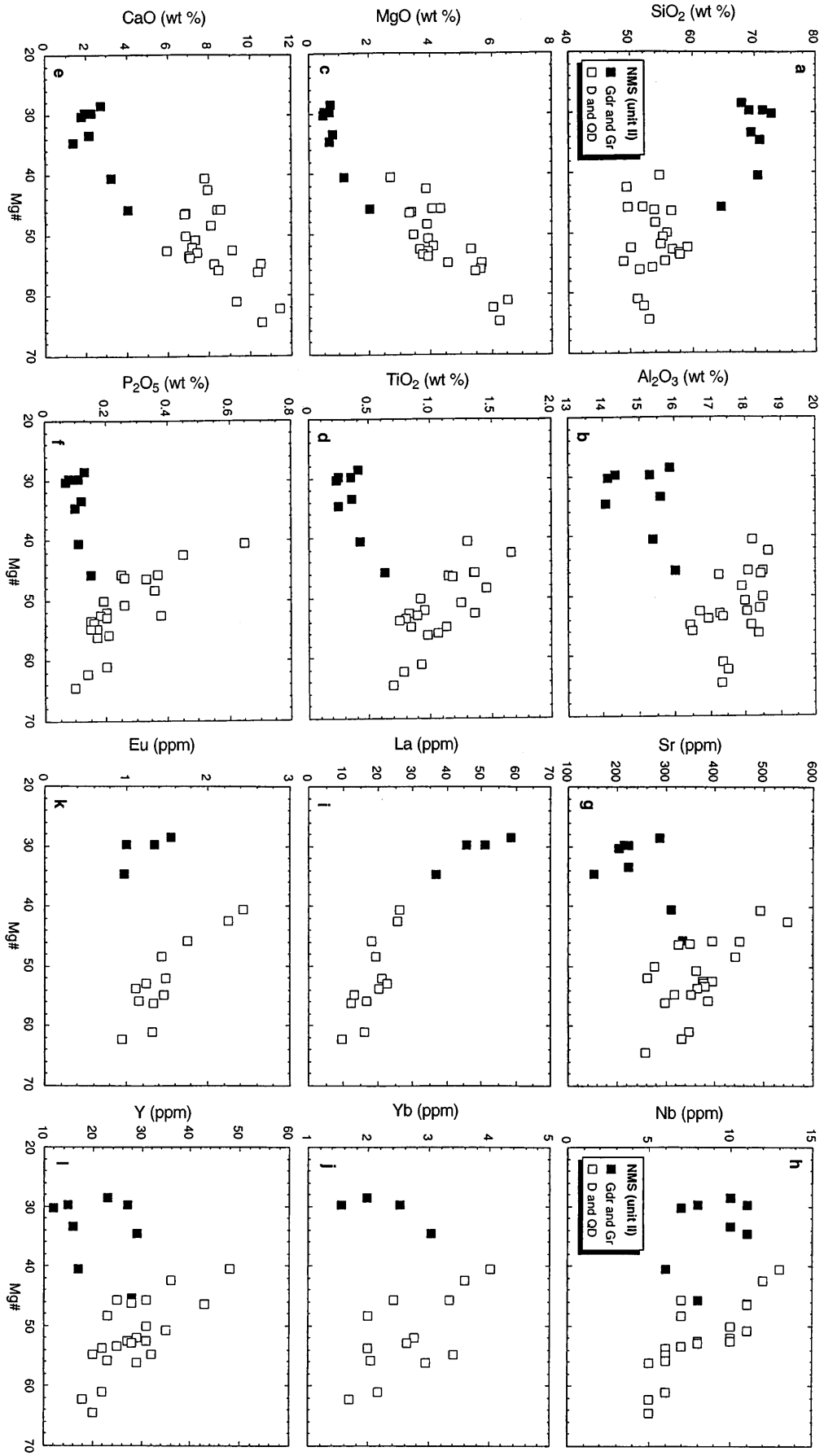

Fig. 7a–l Variations of selected oxides and elements with Mg# [$=100\times$molar $MgO/(MgO+0.9FeO_{tot})$] within the NMS. Note that mafic and felsic samples represent two genetically unrelated fractionation suites

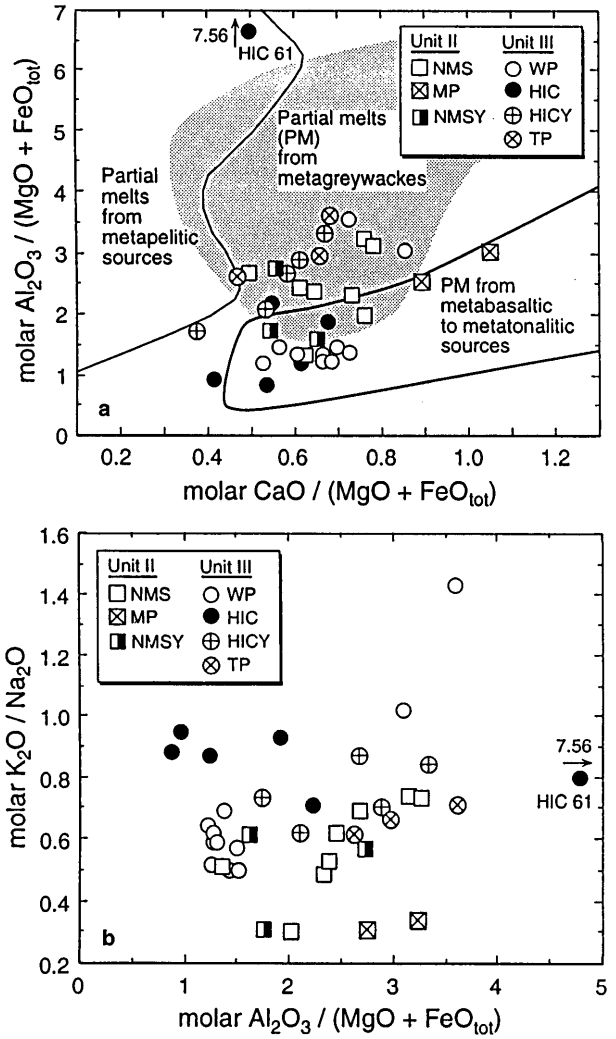

Fig. 8a,b Chemical compositions of I-type granitoids from the Odenwald. **a** Molar $Al_2O_3/(MgO+FeO_{tot})$ vs molar $CaO/(MgO+FeO_{tot})$. *Outlined fields* denote compositions of partial melts obtained in experimental studies by dehydration melting of various bulk compositions (Vielzeuf and Holloway 1988; Conrad et al. 1988; Carroll and Wyllie 1990; Rushmer 1991; Beard and Lofgren 1991; Patiño Douce and Johnston 1991; Skjerlie et al. 1993; Wolf and Wyllie 1994; Beard et al. 1994; Vielzeuf and Montel 1994; Gardien et al. 1995; Skjerlie and Johnston 1996; Patiño Douce and Beard 1995, 1996; Patiño Douce 1996; Singh and Johannes 1996; Thompson 1996; Stevens et al. 1997). See text for further explanation. **b** Molar K_2O/Na_2O vs molar $Al_2O_3/(MgO+FeO_{tot})$. See text for discussion

The felsic (SiO_2–rich) NMS rocks have relatively high abundances of Yb and Sc (Fig. 2l,m), low abundances of Sr (Fig. 2k), and low values of Sr/Y, Sr/Nd, Zr/Y, and $(Tb/Yb)_{cn}$ (Fig. 3). Chondrite-normalized REE patterns of these samples display variable negative Eu anomalies and are characterized by moderate concave-upward shapes (Fig. 5e). These features preclude the involvement of substantial amounts of garnet either in the residue during partial melting or as a part of the fractionating assemblage during an AFC process (DePaolo 1981) in the deeper parts of a thick crust. Instead, plagioclase and amphibole (in addition to clinopyroxene) have to be envisaged as major fractionating phases during magma genesis at relatively shallow depths.

Relative to the older NMS rocks, the younger intrusives of unit II (MP tonalite; NMSY granodioritic and granitic dikes) display similar abundances of large ion lithophile elements (LILE), but higher abundances of Sr (Fig. 2k), lower abundances of Yb and Sc (Fig. 2l,m), and higher ratios of Sr/Y, Sr/Nd, Zr/Y, and $(Tb/Yb)_{cn}$ (Fig. 3). These features, in conjunction with the apparent lack of negative Eu anomalies in the REE patterns (Fig. 5j), suggest an increasing amount of garnet and a decreasing amount of feldspar in the fractionating phase assemblages during magma segregation. This change in the modal compositions of the fractionating assemblages may be explained by an increasing depth of magma segregation and may indicate an increase in the thickness of the crust by basal accretion or underplating. Whereas the NMSY rocks have molar ratios of $Al_2O_3/(MgO+FeO_{total})$, K_2O/Na_2O, and $CaO/(MgO+FeO_{total})$ that are similar to those of the older felsic NMS rocks, the samples from the MP are characterized by higher $CaO/(MgO+FeO_{total})$ and lower K_2O/Na_2O ratios (Fig. 8) suggesting a mafic meta-igneous, rather than a meta-graywacke, source. This hypothesis of different source rock compositions is further substantiated by the higher $\varepsilon_{Nd}(I)$ and lower $\delta^{18}O$ values of the MP as compared with the felsic NMS rocks (Fig. 6c,e).

Genesis of unit-III magmas

Common features of most unit-III rocks (WP, WPE, TP, HICY) are relatively high abundances of LILE, low abundances of Yb and Sc (Fig. 2), and high values of Sr/Y, Sr/Nd, Zr/Y, and $(Tb/Yb)_{cn}$ (Fig. 3). Chondrite-normalized REE patterns of samples from the TP, WP, and HICY suites are characterized by significant LREE/HREE and MREE/HREE fractionations and the apparent lack of Eu anomalies (Fig. 5f,i,k). All these features indicate that garnet was a major fractionating phase and that fractionation of plagioclase was limited. The HIC rocks also have elevated abundances of K, Rb, and Pb (Fig. 2g–i), but otherwise show characteristics that are more similar to those of the older unit-II (NMS) rocks, suggesting somewhat higher degrees of feldspar and lower degrees of garnet fractionation. The younger HICY granites, however, display the highest $(Tb/Yb)_{cn}$ and Zr/Y values of all Odenwald granitoids (Fig. 3b,c) and show no Eu anomalies (Fig. 5k) suggesting that garnet played a dominant and plagioclase an insignificant role during magma segregation.

As for the felsic rocks of unit II, the $Al_2O_3/(MgO+FeO_{total})$ vs $CaO/(MgO+FeO_{total})$ relationships preclude an origin of the felsic unit-III magmas from a metapelitic source (Fig. 8a). Whereas a meta-

basaltic to metatonalitic source seems most appropriate for the HIC and WP magmas, the higher $Al_2O_3/(MgO + FeO_{total})$ ratios of the younger TP and HICY rocks suggest derivation from an Al-poor metagraywacke source.

The WPE samples included in this study were all taken from the central parts of large (meter-sized) mafic microgranular enclaves within the WP host rock. Field relationships and rock textures suggest that these enclaves originated from globules of mafic magma which mingled with and chilled against the felsic host magma. We assume that these samples represent primary magma compositions that were not modified by chemical exchange between enclave and host magmas. Relative to the mafic NMS rocks of unit II, the WPE samples are characterized by lower abundances of CaO, Yb, and Sc, but higher abundances of Na_2O, K_2O, Rb, Pb, and Sr (Fig. 2). Furthermore, the WPE samples show higher values of Sr/Y, Zr/Y, and $(Tb/Yb)_{cn}$ (Fig. 3) and higher abundances of the high field strength elements Ti, P, Zr, Hf, Nb, and Ta (Fig. 9). Such features are typical of rocks belonging to the shoshonitic (monzonitic) series (Fig. 2g). Relatively high values of Mg# (60 to 48) in combination with low contents of SiO_2 (48.7–60.0 wt.%; most samples <55.0 wt.%) and moderate Na_2O contents (3.1–4.9 wt.%) preclude an origin of the WPE magmas by dehydration melting from normal mafic lower crust. Instead, these magmas were probably derived from a relatively deep-seated enriched lithospheric mantle domain. An origin from an enriched mantle source is also substantiated by the isotopic signatures of one representative WPE sample (Fig. 6; Table 3).

Tectonic setting of Odenwald intrusive magmatism

Variscan plutonism in the Odenwald which is located at the northern edge of the MGCR could be either subduction related or syncollisional. At present, there are poor constraints on the duration of south-directed subduction beneath the Saxothuringian domain (Armorica) and the final closure of the Rhenohercynian ocean (Fig. 1, inset). The culmination of high-P/low-T metamorphism in the Northern Phyllite zone and southern Rhenohercynian zone must be slightly older than ~328 Ma (Ahrendt et al. 1983; Massonne 1995). In the lower (parautochthonous) units of the Rhenohercynian zone (East Avalonia) synorogenic sedimentation started at latest during the Early Carboniferous IIδ/IIIα (i.e., ~335 Ma ago; Gradstein and Ogg 1996). This period, therefore, represents an upper time limit for the emplacement of allochthonous flysch units derived from the northern margin of Armorica (e.g., the Giessen-Harz nappe) and, hence, for the closure of the Rhenohercynian ocean (Franke 1995). Therefore, the ~362-Ma-old FGC (unit I) must have been generated at least 20 Ma before the Rhenohercynian ocean was closed, most likely in an arc-type setting. For the ~340- to 335-Ma-old magmatic rocks from units II and III, a syncollisional, rather than an arc-type setting, has to be envisaged.

Numerous studies suggest that trace elements may serve to discriminate between different tectonic settings of granitoid magmas. Pearce et al. (1984), for example, demonstrated that the Rb–Y–Yb–Nb(–Ta) space is most effective in identifying ocean-ridge granitoids (ORG), volcanic-arc granitoids (VAG), within-plate granitoids (WPG), and syn-collisonal granitoids (syn-COLG). Applying their discrimination criteria, the Odenwald intrusive rocks are all classified as VAG (Fig. 10a–c). In all diagrams, granitoids from unit III plot nearer to the field of syn-COLG than those from units I and II. Furthermore, there is a temporal evolution within unit II with the younger MP tonalite sample(s) and the NMSY dike rocks plotting nearer to the field of syn-COLG than the older NMS rocks. Harris et al. (1986) studied chemical characteristics of collision-related granitoid rocks and used Rb–Hf–Ta relationships to distinguish volcanic-arc or pre-collisional (pre-COLG), syn-collisional, and post-collisional granitoids. Using their discriminating frame, the Odenwald rocks classify as pre-COLG or VAG (Fig. 10d). Again, rocks from unit III plot nearer to the fields of syn-COLG and post-COLG than those from units I and II. Further arguments in favor of a volcanic-arc nature of the Odenwald granitoids derive from their Rb/Cs and Rb/Zr values. Similar to arc magmas (Hart and Reid 1991), the Odenwald granitoids display low ratios of Rb/Cs (≤ 56). Low Rb/Zr values (<1.1) in almost all samples, with only some granites from the HIC and TP suites (unit III) showing slightly higher values (up to 2.9), are also compatible with a pre-collisional or volcanic-arc nature (Harris et al. 1986).

It should, however, be kept in mind that conclusions drawn from tectonic discrimination diagrams are ambiguous, as trace element signatures of magmas are also dependent on protolith composition (e.g., Roberts and Clemens 1993). Therefore, we conclude that (a) the chemical signatures of the FGC rocks suggest an arc-type setting of unit I at ~362 Ma B.P. (Famennian), and (b) the compositions of the younger (~340–335 Ma) granitoids from units II and III allow for, but do not necessarily demand, a subduction-related origin. In any case, the chemical data suggest an evolution from a more subduction-related to a more syn-collisional nature of the magmas, which is in line with geological constraints.

Crystallization pressures obtained by Al-in-hornblende barometry (Table 1) imply significant syn- to post-intrusive vertical displacements between units I, II, and III. Kinematic indicators suggest divergent sinistral strike-slip movements within unit II and between units I, II, and III during and after the emplacement of unit-II magmas, i.e., between approximately 340 and 335 Ma (Krohe 1991, 1992, Krohe and Willner 1995). An overall transtensional setting during this time span is also compatible with the chemical nature of unit-III

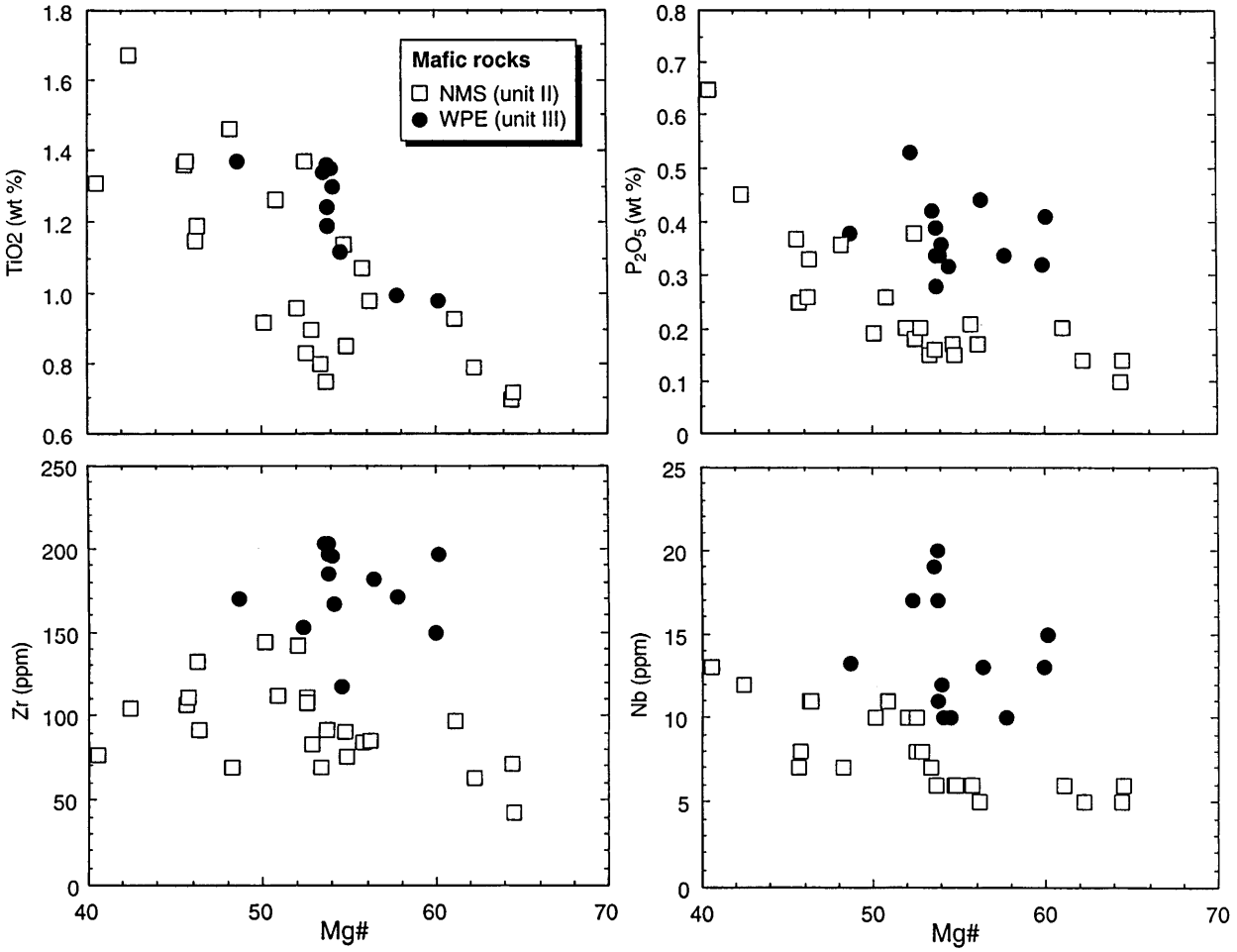

Fig. 9 Variations of some high field strength elements (HFSE) with Mg# [$=100\times$molar MgO/(MgO + 0.9FeO$_{tot}$)] within the mafic rocks from the NMS (unit II) and WPE (unit III) suites. Note that the WPE samples tend to have higher abundances of HFSE than the NMS rocks

magmas which belong to the shoshonitic series (Fig. 2g). It has repeatedly been suggested that shoshonitic/monzonitic magmatism occurs during the termination of an oblique subduction phase and coincident with the onset of arc extension (e.g., Morrison 1980; Rapela and Pankhurst 1996, and references therein).

Contribution of Avalonian material to the felsic Odenwald magmas?

It has been suggested that the various tectonic blocks forming the MGCR can be assigned to two groups with different tectonic identity. Most of the Saxothuringian (Armorican) units (e.g., units I–III from the Odenwald) should be underlain by tectonically underplated Rhenohercynian (Avalonian) material, whereby unit IV of the Odenwald (Böllstein Odenwald) and the entire Spessart (Fig. 1) are thought to represent such basally accreted fragments (Oncken 1997). As time constraints suggest a syncollisional nature of the granitoids from units II and III, a contribution from underplated Avalonian material to the felsic granitoids has to be envisaged.

Recent studies on the Sm–Nd isotopic systematics of the Rhenohercynian units (Küstner et al. 1999) reveal that both the parautochthonous passive-margin sequences (Old Red Continent, Avalonia) and the nappes derived from the northern margin of the Saxothuringian domain (Armorica) have ε_{Nd} (340 Ma) values that are considerably lower than those of the Odenwald granitoids. A significant contribution of underplated Rhenohercynian graywackes to the Odenwald magmas can therefore be ruled out. Felsic metaigneous rocks from unit IV of the Odenwald and from equivalent units of the Spessart (Rotgneiss and Haibach gneiss) can also be excluded as possible sources for the Odenwald magmas, because these rocks display high $^{87}Sr/^{86}Sr$ (340–335 Ma) ratios (0.710–0.715) and peraluminous compositions (Lippolt 1986; Altenberger and Besch 1993; Anthes and Reischmann 1995; Dombrowski et al. 1995; Reischmann et al. 1999). Volumetrically less abundant amphibolites and related metaluminous gneisses from the Böllstein Odenwald and the Spessart represent the only possible Avalonian

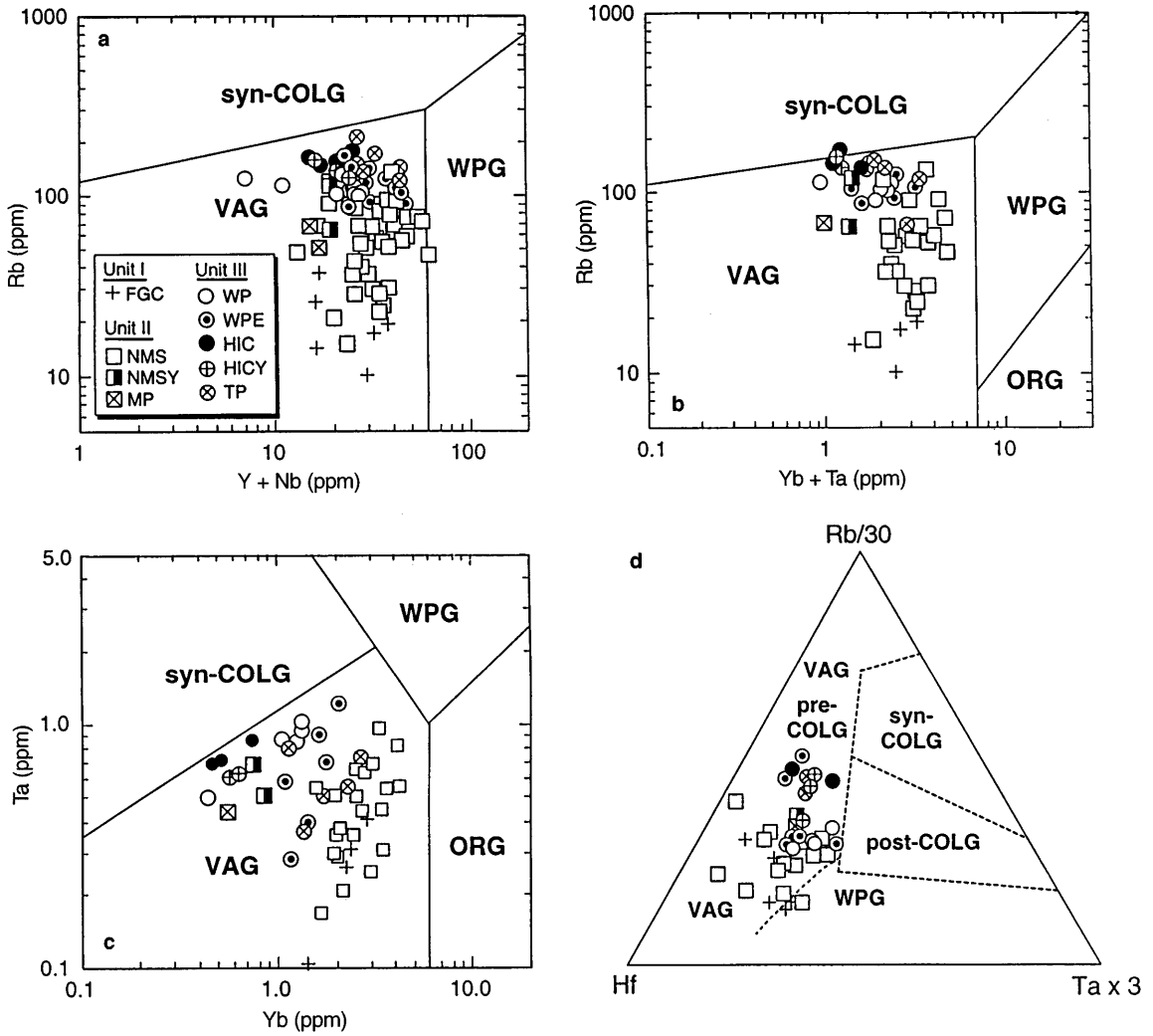

Fig. 10a–d Chemical compositions of granitoids from the Odenwald in tectonic discrimination diagrams with fields of within-plate granitoids (*WPG*), volcanic-arc granitoids (*VAG*) or pre-collisional granitoids (*pre-COLG*), syn-collisional granitoids (*syn-COLG*) and post-collisional granitoids (*post-COLG*). **a–c** Rb vs (Y + Nb), Rb vs (Yb + Ta) and Ta vs Yb discrimination diagrams of Pearce et al. (1984). **d** Rb–Hf–Ta triangular plot of Harris et al. (1986)

protoliths for the felsic granitoids from units II and III. These mafic rocks show chemical characteristics similar to island-arc basalts (Altenberger et al. 1990; Okrusch 1995). As yet, no isotopic data are available for these rocks.

Possible equivalents of the Odenwald granitoids in other parts of the Saxothuringian domain

The initial isotopic signatures and chemical characteristics of the syncollisional Odenwald granitoids (units II and III) are similar to those of contemporaneous granitoids from other parts of the Saxothuringian domain. In the northern Vosges and Schwarzwald (Fig. 1 inset), early high-K I-type diorites, granodiorites, and granites are followed by shoshonitic granites (Altherr et al., in press). Using the tectonic frame of Edel and Weber (1995), the Central Bohemian batholith (CBB) is in an equivalent position to the plutons of the northern Vosges and northern Schwarzwald. For the CBB, U–Pb single-zircon dating by stepwise evaporation has established that successive intrusions were emplaced between approximately 351 ± 11 and 343 ± 6 Ma (Holub et al. 1997), whereby an evolution from early medium-K to later high-K and monzonitic magmas with more evolved isotopic signatures is observed (Janousek et al. 1995).

Conclusions

The results of this study allow for the following major conclusions:

1. Latest Devonian to early Carboniferous plutonism of the Odenwald documents the transition from subduction to collision. The ~362-Ma-old Franken-

stein gabbroic complex (FGC) in the northernmost tectonometamorphic unit I was generated as a part of a magmatic arc during oblique south- to SSW-directed subduction of oceanic lithosphere (Rhenohercynian ocean). During oblique collision between East Avalonia (Rhenhercynian domain) and Armorica (Saxothuringian domain) at 340–335 Ma B.P., normal to high-K (unit II) and high-K to monzonitic magmas (unit III) were emplaced in a transtensional setting.

2. The FGC magmas (unit I) were derived from a relatively shallow depleted mantle source metasomatized by subduction-related H_2O-rich fluids. A contribution from the continental crust cannot be detected.
3. The NMS of unit II comprises two different magma series for which a comagmatic relationship can be excluded. Mafic NMS rocks represent variably fractionated melts derived from a relatively shallow enriched mantle source. For the volumetrically subordinate felsic NMS rocks an origin by dehydration melting of metaluminous crustal protoliths (metagraywacke, metabasalt, metatonalite) seems most plausible. Trace element signatures suggest a relatively shallow depth of magma segregation. Trace element characteristics of the younger intrusives from unit II (MP, NMSY), however, suggest a greater depth of magma segregation from metaluminous mafic meta-igenous (MP) or metagraywacke (NMSY) sources.
4. Mafic and felsic magmas of the shoshonitic/monzonitic series emplaced in unit III (WP, WPE, HIC, HICY, TP) suggest the termination of oblique subduction and increasing arc extension. Trace element and isotopic signatures of the mafic rocks are best explained by a deep-seated enriched (lithospheric) mantle source. Higher initial Sr ratios and $\delta^{18}O$ values in conjunction with high Sr/Y, Zr/Y, and $(Tb/Yb)_{cn}$ ratios of the felsic rocks suggest a substantial contribution from a garnet-rich crustal source.
5. The chemical and isotopic characteristics of the Odenwald granitoids do not support the hypothesis that large parts of the MGCR are underlain by tectonically underplated Avalonian material.

Acknowledgements This study is a contribution to the German National Research Project "Orogenic Processes with particular reference to the Variscides". Financial support by "Deutsche Forschungsgemeinschaft" (Al 166/8) is gratefully acknowledged. Technical support was provided by H. Frohna-Binder, R. Gehann, H.-P. Meyer, C. Wacker (†), and H. Marschall. We thank G. Eisbacher, A. Holl, B. Kreher, A. Krohe, F. Volker, and A. Willner for discussions, A. Kalt for comments on previous versions of the manuscript, and S. Jung and M. P. Roberts for constructive reviews.

References

Ahrendt H, Clauer N, Hunziker JC, Weber K (1983) Migration of folding and metamorphism in the Rheinisches Schiefergebirge deduced from K–Ar and Rb–Sr age determinations. In: Martin H, Eder FW (eds) Intracontinental Fold Belts. Springer, Berlin Heidelberg New York, pp 323–338

Ahrendt, H, Franzke HJ, Marheine D, Schwab M, Wemmer K (1996) Zum Alter der Metamorphose in der Wippraer Zone/Harz – Ergebnisse von K/Ar-Altersdatierungen an schwachmetamorphen Sedimenten. Z Dtsch Geol Ges 147:11–28

Altenberger U, Besch T (1993) The Böllstein Odenwald: Evidence for a pre- to early Variscan plate convergence in the Central European Variscides. Geol Rundsch 82:475–488

Altenberger U, Besch T, Mocek B, Zaipeng Y, Yong S (1990) Geochemie und Geodynamik des Böllsteiner Odenwaldes. Mainzer Geowiss Mitt 1990:183–200

Altherr R, Lugovic B, Meyer H-P, Majer V (1995) Early Miocene post-collisional calc-alkaline magmatism along the easternmost segment of the Periadriatic fault system (Slovenia and Croatia). Mineral Petrol 54:225–247

Altherr R, Holl A, Hegner E, Langer C, Kreuzer H (in press) High-potassium, calc-alkaline I-type plutonism in the European Variscides: northern Vosges (France) and northern Schwarzwald (Germany). Lithos

Anderle HJ, Massonne H-J, Meisl J, Oncken O, Weber K (1990) Southern Taunus Mountains. Terranes in the Circum-Atlantic Paleozoic Orogens (IGCP 233), Field Guide: Rhenohercynian Belt and Mid-German Crystalline Rise, pp 125–148, Göttingen

Anthes G, Reischmann T (1995) Regional variations of Nd and Sr isotopes of the Mid German Crystalline Rise. Terra Nostra 95/8:78

Atherton MP, Petford N (1993) Generation of sodium-rich magmas from newly underplated basaltic crust. Nature 362:144–146

Beard JS, Lofgren E (1991) Dehydration melting and water-saturated melting of greenstone and amphibolite at 1, 3 and 6.9 kb. J Petrol 32:365–401

Beard JS, Lofgren E, Sinha AK, Tollo RP (1994) Partial melting of apatite-bearing charnockite, granulite, and diorite: melt compositions, restite mineralogy and petrologic implications. J Geophys Res 99:21591–21603

Boynton WV (1984) Cosmochemistry of the rare earth elements: meteorite studies. In: Henderson P (ed) Rare earth element geochemistry. Elsevier, Amsterdam, pp 63–114

Carroll MR, Wyllie PJ (1990) The system tonalite-H_2O at 15 kbar and the genesis of calc-alkaline magmas. Am Mineral 75:345–357

Class C, Altherr R, Volker F, Eberz G, McCulloch MT (1994) Petrogenesis of Pliocene to Quaternary alkali basalts from the Huri Hills, northern Kenya. Chem Geol 113:1–22

Conrad WK, Nicholls IA, Wall VJ (1988) Water-saturated and -undersaturated melting of metaluminous and peraluminous crustal compositions at 10 kbar: evidence for the origin of silicic magmas in the Taupo Volcanic Zone, New Zealand, and other occurrences. J Petrol 29:765–803

DePaolo DJ (1981) Trace element and isotopic effects of combined wall rock assimilation and fractional crystallization. Earth Planet Sci Lett 53:189–202

Dombrowski A, Henjes-Kunst F, Höhndorf A, Kröner A, Okrusch M, Richter P (1995) Orthogneisses in the Spessart Crystalline Complex, north-west Bavaria: Silurian granitoid magmatism at an active continental margin. Geol Rundsch 84:399–411

Edel JB, Weber K (1995) Cadomian terranes, wrench faulting and thrusting in the central Europe Variscides: geophysical and geological evidence. Geol Rundsch 84:412–432

Finger F, Roberts MP, Haunschmid B, Schermaier A, Steyrer HP (1997) Variscan granitoids of central Europe: their typology, potential sources and tectonothermal relations. Mineral Petrol 61:67–96

Franke W (1995) III.B.1 Stratigraphy. In: Dallmeyer RD, Franke W, Weber K (eds) Pre-Permian geology of central and eastern Europe, IGCP 233. Springer, Berlin Heidelberg New York, pp 34–49

Friedrich G (1955) Petrographie und Tektonik des Melibokus-Massivs. Aufschluss 2:35–40

Ganssloser M, Theye T, Wachendorf H (1996) Detrital glaucophane in graywackes of the Rhenohercynian Harz mountains and the geodynamic implications. Geol Rundsch 85:755–760

Gardien V, Thompson AB, Grujic D, Ulmer P (1995) Experimental melting of biotite + plagioclase + quartz ± muscovite assemblages and implications for crustal melting. J Geophys Res 100:15581–15591

Gradstein FM, Ogg J (1996) A Phanerozoic time scale. Episodes 19:3–5

Harris NBW, Pearce JA, Tindle AG (1986) Geochemical characteristics of collision-zone magmatism. In: Coward MP, Ries AC (eds) Collision tectonics. Geol Soc Lond Spec Publ 19:67–81

Hart SR, Reid MR (1991) Rb/Cs fractionation: a link between granulite metamorphism and the S-process. Geochim Cosmochim Acta 55:2379–2383

Hegner E, Roddick CR, Fortier SM, Hulbert L (1995) Nd, Sr, Pb, Ar and O isotope systematics of Sturgeon Lake kimberlite, Saskatchewan, Canada: constraints on emplacement age, alteration, and source composition. Contrib Mineral Petrol 120:212–222

Hellmann K-N (1975) Die Granodioritporphyrite des Bergsträsser Odenwaldes. Aufschluss 27:189–196

Hellmann K-N, Emmermann R, Lippolt HJ (1975) Stoffbestand der Granodioritporphyrite des Bergsträsser Odenwaldes. N Jahrb Mineral Abh 123:253–274

Hellmann K-N, Lippolt HJ, Todt W (1982) Interpretation der Kalium-Argon-Alter eines Odenwälder Granodioritporphyritganges und seiner Nebengesteine. Aufschluss 33:155–164

Henes-Klaiber U, Holl A, Altherr R (1989) The Odenwald: more evidence for Hercynian arc magmatism. Terra Abstr 1:281

Hess JC, Schmidt G (1989) Zur Altersstellung der Kataklasite im Bereich der Otzberg-Zone, Odenwald. Geol Jahrb Hessen 117:69–77

Hildreth W, Moorbath S (1988) Crustal contributions to arc magmatism in the Andes of Central Chile. Contrib Mineral Petrol 98:455–489

Holub FV, Cocherie A, Rossi P (1997) Radiometric dating of granitic rocks from the Central Bohemian Plutonic Complex (Czech Republic): constraints on the chronology of thermal and tectonic events along the Moldanubian–Barrandian boundary. C R Acad Sci Paris 325:19–26

Janousek V, Rogers G, Bowes DR (1995) Sr–Nd isotopic constraints on the petrogenesis of the Central Bohemian Pluton, Czech Republic. Geol Rundsch 84:521–534

Keppler H (1996) Constraints from partitioning experiments on the composition of subduction-zone fluids. Nature 380:237–240

Kirsch H, Kober B, Lippolt HJ (1988) Age of intrusion and rapid cooling of the Frankenstein gabbro (Odenwald, SW-Germany) evidenced by $^{40}Ar/^{39}Ar$ and single-zircon $^{207}Pb/^{206}Pb$ measurements. Geol Rundsch 77:639–711

Kossmat F (1927) Gliederung des varistischen Gebirgsbaus. Abh Sächs Geol Landesamt 1:1–39

Kreher B (1994) Petrologie und Geochemie der Gabbrointrusionen des Frankensteins (Odenwald) Geol Jahrb Hessen 122:81–122

Kreuzer H, Harre W (1975) K/Ar-Altersbestimmungen an Hornblenden und Biotiten des kristallinen Odenwaldes. Aufschluss 27:71–78

Krohe A (1991) Emplacement of synkinematic plutons in the Variscan Odenwald (Germany) controlled by transtensional tectonics. Geol Rundsch 80:391–409

Krohe A (1992) Structural evolution of intermediate-crustal rocks in a strike-slip and extensional setting (Variscan Odenwald, SW Germany): differential upward transport of metamorphic complexes and changing deformation mechanisms. Tectonophysics 206:357–386

Krohe A (1994) Verformungsgeschichte in der mittleren Kruste eines magmatischen Bogens – der variszische Odenwald als Modellregion. Geotekton Forsch 80:1–152

Krohe A (1996) Variscan tectonics of central Europe: postaccretionary intraplate deformation of weak continental lithosphere. Tectonics 15:1364–1388

Krohe A, Willner AP (1995) IV.C.2. The Odenwald Crystalline Complex. In: Dallmeyer RD, Franke W, Weber K (eds) Pre-Permian geology of central and eastern Europe, IGCP 233. Springer, Berlin Heidelberg New York, pp 174–181

Küstner W, Ahrendt H, Hansen BT, Wemmer K (1999) K–Ar cooling ages of detrital muscovites and Sm–Nd model ages of pre- and synorogenic low metamorphic sediments of the Rhenohercynian zone: fundamental data for a quantification of orogenic processes with particular reference to the Variscides. Terra Nostra 99/1:135

Lippolt HJ (1986) Nachweis altpaläozoischer Primäralter (Rb/Sr) und karbonischer Abkühlungsalter (K/Ar) der Muskovit-Biotit-Gneise des Spessarts und der Biotit-Gneise des Böllsteiner Odenwaldes. Geol Rundsch 75:569–583

Lippolt HJ, Kirsch H (1994) Ar^{40}/Ar^{39}–Untersuchungen an serizitisierten Plagioklasen des Frankenstein-Gabbros (NW-Odenwald) in Hinblick auf ihren Alterations-Zeitpunkt. Geol Jahrb Hessen 122:123–142

Maggetti M (1971) Die basischen Intrusiva des Heppenheim-Lindenfelser Zuges (Mittlerer Bergsträsser Odenwald), Teil I und II. N Jahrb Mineral Abh 115:192–251

Maggetti M (1974) Zur Dioritbildung im kristallinen Odenwald. Schweiz Mineral Petrogr Mitt 54:39–57

Maggetti M (1975) Die Tiefengesteine des Bergsträsser Odenwaldes. Aufschluss 27:87–108

Maggetti M, Nickel E (1973) Hornblende-Diorite und Biotit-Diorite im kristallinen Odenwald. N Jahrb Mineral Abh 119:232–265

Massone H-J (1995) III.C.4 Metamorphic evolution. In: Dallmeyer RD, Franke W, Weber K (eds) Pre-Permian geology of central and eastern Europe, IGCP 233. Springer, Berlin Heidelberg New York, pp 132–137

Matthes S, Okrusch M, Richter P (1972) Zur Migmatit-Bildung im Odenwald. N Jahrb Mineral Abh 116:225–267

Matthes S, Schubert W (1971) Der Original-Beerbachit im Odenwald, ein Amphibolit-Hornfels in Pyroxen-Hornfelsfazies. Contrib Mineral Petrol 33:62–86

Meisl S (1970) Petrologische Studien im Grenzbereich Diagenese-Metamorphose. Abh Hess L-A f Bodenforschung 57:1–93

Meisl S (1990) Metavolcanic rocks in the "Northern Phyllite Zone" at the southern margin of the Rhenohercynian Belt. Terranes in the Circum-Atlantic Paleozoic Orogens (IGCP 233). Field Guide: Rhenohercynian Belt and Mid-German Crystalline Rise, pp 25–42, Göttingen

Meisl S, Anderle H-J, Strecker G (1982) Niedrigtemperierte Metamorphose im Taunus und im Soonwald. Fortschr Mineral 60 Beih 2:43–69

Morrison GW (1980) Characteristics and tectonic setting of the shoshonitic rock association. Lithos 13:97–108

Nickel E, Fettel M (1985) Odenwald. Vorderer Odenwald zwischen Darmstadt und Heidelberg. Sammlung Geol. Führer 65, Gebr Borntaeger, Berlin, Stuttgart

Nickel E, Maggetti M (1974) Magmenentwicklung und Dioritbildung im synorogen konsolidierten Grundgebirge des Bergsträsser Odenwaldes. Geol Rundsch 63:618–654

Okrusch M (1995) IV.E Metamorphic evolution. In: Dallmeyer RD, Franke W, Weber K (eds) Pre-Permian geology of central and eastern Europe, IGCP 233. Springer, Berlin Heidelberg New York, pp 201–213

Oncken O (1997) Transformation of a magmatic arc and an orogenic root during oblique collision and its consequences for the evolution of the European Variscides (Mid-German Crystalline Rise). Geol Rundsch 86:2–20

Patiño Douce AE (1996) Effects of pressure and H_2O content on the composition of primary crustal melts. Trans R Soc Edinburgh Earth Sci 87:11–21

Patiño Douce AE, Beard JS (1995) Dehydration-melting of biotite gneiss and quartz amphibolite from 3 to 15 kbar. J Petrol 36:707–738

Patiño Douce AE, Beard JS (1996) Effects of P, f(O_2) and Mg/Fe ratio on dehydration melting of model metagreywackes. J Petrol 37:999–1024

Patiño Douce AE, Johnston AD (1991) Phase equilibria and melt productivity in the pelitic system: implications for the origin of peraluminous granitoids and aluminous granulites. Contrib Mineral Petrol 107:202–218

Pearce JA, Harris NB, Tindle AG (1984) Trace element discrimination for the tectonic interpretation of granitic rocks. J Petrol 25:956–983

Peccerillo A, Taylor SR (1976) Geochemistry of Eocene calc-alkaline volcanic rocks from the Kastamonu area, northern Turkey. Contrib Mineral Petrol 58:63–81

Rapela CW, Pankhurst RJ (1996) Monzonite suites: the innermost Cordilleran plutonism of Patagonia. Trans R Soc Edinburgh Earth Sci 87:193–203

Rapp RP (1995) Amphibole-out phase boundary in partially melted metabasalt, its control over liquid fraction and composition, and source permeability. J Geophys Res 100:15601–15610

Rapp RP, Watson EB (1995) Dehydration melting of metabasalt at 8–32 kbar: implications for continental growth and crust-mantle recycling. J Petrol 36:891–931

Reischmann T, Anthes G, Jaeckel P (1999) Age and origin of the Böllsteiner Odenwald. Terra Nostra 99/1:166

Roberts MP, Clemens JD (1993) Origin of high-potassium, calc-alkaline, I-type granitoids. Geology 21:825–828

Romick JD, Kay SM, Kay RW (1992) The influence of amphibole fractionation on the evolution of calcalkaline andesite and dacite tephra from the central Aleutians, Alaska. Contrib Mineral Petrol 112:101–118

Rushmer T (1991) Partial melting of two amphibolites: contrasting experimental results under fluid-absent conditions. Contrib Mineral Petrol 107:41–59

Schaltegger U (1997) Magma pulses in the central Variscan belt: episodic melt generation and emplacement during lithospheric thinning. Terra Nova 9:242–245

Schmidt MW (1992) Amphibole composition in tonalite as a function of pressure: an experimental calibration of the Al-in-hornblende barometer. Contrib Mineral Petrol 110:304–310

Siedel H, Theye T (1993) Very low grade metamorphism of pelites in the Wippra metamorphic Zone, Harz Mountains, Germany. N Jahrb Mineral Mh 1993:115–132

Singh J, Johannes W (1996) Dehydration melting of tonalites. Part II. Composition of melts and solids. Contrib Mineral Petrol 125:26–44

Skjerlie KP, Johnston AD (1996) Vapour-absent melting from 10 to 20 kbar of crustal rocks that contain mutiple hydrous phases: implications for anatexis in the deep to very deep continental crust and active continental margins. J Petrol 37:661–691

Skjerlie KP, Patiño Douce AE, Johnston AD (1993) Fluid absent melting of a layered crustal protolith: implications for the generation of anatectic granites. Contrib Mineral Petrol 114:365–378

Stevens G, Clemens JD, Droop GTR (1997) Melt production during granulite-facies anatexis: experimental data from "primitive" metasedimentary protoliths. Contrib Mineral Petrol 128:352–370

Taylor SR, McLennan SM (1985) The continental crust: its composition and evolution. Blackwell, Oxford,

Thompson AB (1996) Fertility of crustal rocks during anatexis. Trans R Soc Edinburgh Earth Sci 87:1–10

Todt WA, Altenberger U, Raumer JF von (1995) U–Pb data on zircons for the thermal peak of metamorphism in the Variscan Odenwald, Germany. Geol Rundsch 84:466–472

Trochim HD (1955) Der Gabbro vom Frankenstein. Aufschluss 2:41–47

Vennemann TW, Smith HS (1990) The rate and temperature of reaction of ClF3 with silicate minerals, and their relevance to oxygen isotope analysis. Chem Geol 86:83–88

Vielzeuf D, Holloway JR (1988) Experimental determination of fluid-absent melting relations in the pelitic system. Contrib Mineral Petrol 98:357–276

Vielzeuf D, Montel JM (1994) Partial melting of metagreywackes. 1. Fluid-absent experiments and phase relationships. Contrib Mineral Petrol 117:375–393

White WM, Dupré B (1986) Sediment subduction and magma genesis in the lesser Antilles: isotopic and trace element constraints. J Geophys Res 91:5927–5941

Willner AP, Massone H-J, Krohe A (1991) Tectono-thermal evolution of a part of a Variscan magmatic arc: the Odenwald in the Mid-German Crystalline Rise. Geol Rundsch 80:369–389

Wolf MB, Wyllie JP (1994) Dehydration-melting of amphibolite at 10 kbar: the effects of temperature and time. Contrib Mineral Petrol 115:369–383